2019

Structural investigations using theoretical approaches : a study of metal halides, borylenes, phenalenyl complexes and σ-hole interactions

Supreeth Prasad
University of Richmond

Structural Investigations Using Theoretical Approaches

A Study of Metal Halides, Borylenes, Phenalenyl Complexes and σ-Hole Interactions

By
Supreeth Prasad

Honors Thesis

Submitted to:

Department of Chemistry
University of Richmond
Richmond, Virginia 23173
April 2019

Advisor: Dr. Kelling Donald

To Dr. Kelling J. Donald,

I hope to finally have made you proud. You have been an amazing mentor since the beginning. You helped me whenever I had problems, be it personal, academic or professional. Your sage-like advice has helped me grow as a student and as a person. I feel that every interaction I have with you, I learn something new.

"*All the secrets of the world are contained in books. Read at your own risk*."
-Lemony Snicket

Acknowledgements

The information contained within this work has been supported by the National Science Foundation and NSF-MRI Grants, the University of Richmond and the MERCURY consortium. The author is indebted to Dr. Kelling J. Donald for support as a teacher, mentor, and reviewer. This work serves to further investigations into noncovalent interactions and the structural preferences of organic and inorganic systems. The author is grateful to the work done not only by Kelling Donald, but also by Ezana Befekadu, Bernard Wittmaack, László von Szentpály and Roald Hoffmann.

Chapter 1

Bending Ternary Halides

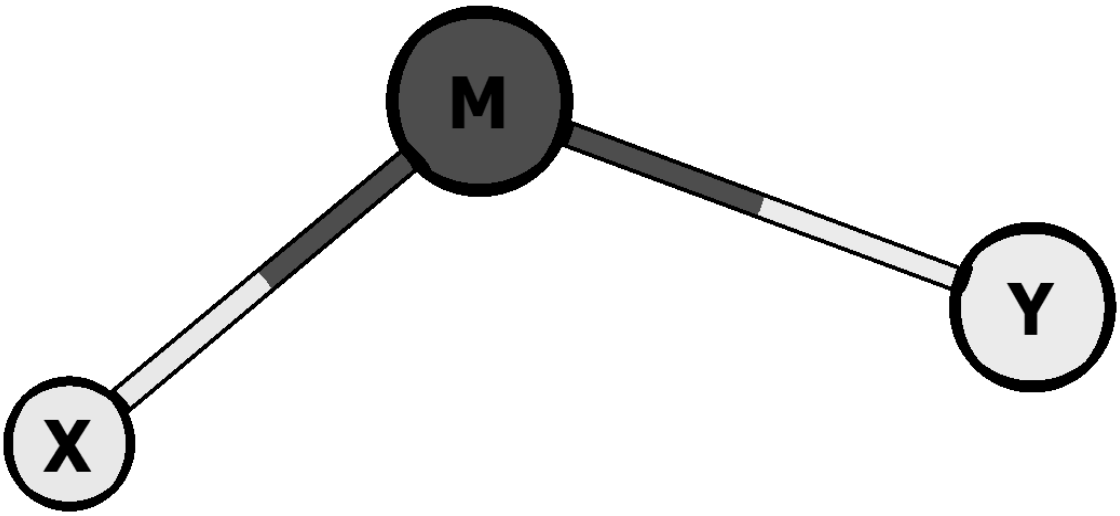

Abstract

The anomalous bending in the group 2 binary dihalides and the absence of this behavior in group 12 systems is well established. Their structural preferences contradict simple bonding models, yet they have received little to no attention in the literature. In this work, for the first time, the gas phase structural preferences of the groups 2 and 12 mixed (ternary) dihalides MXY (M = Be, Mg, Ca, Sr, Ba, Ra, Zn, Cd and Hg, and X, Y = F, Cl, Br, I, At) are investigated at high levels of theory. I extend a previously established softness criterion for bending to the mixed systems and I find that for all bent molecules, for each metal, functions of the form $E(\Theta) = Ae^{-k\Theta}$ predict their barrier to linearization.

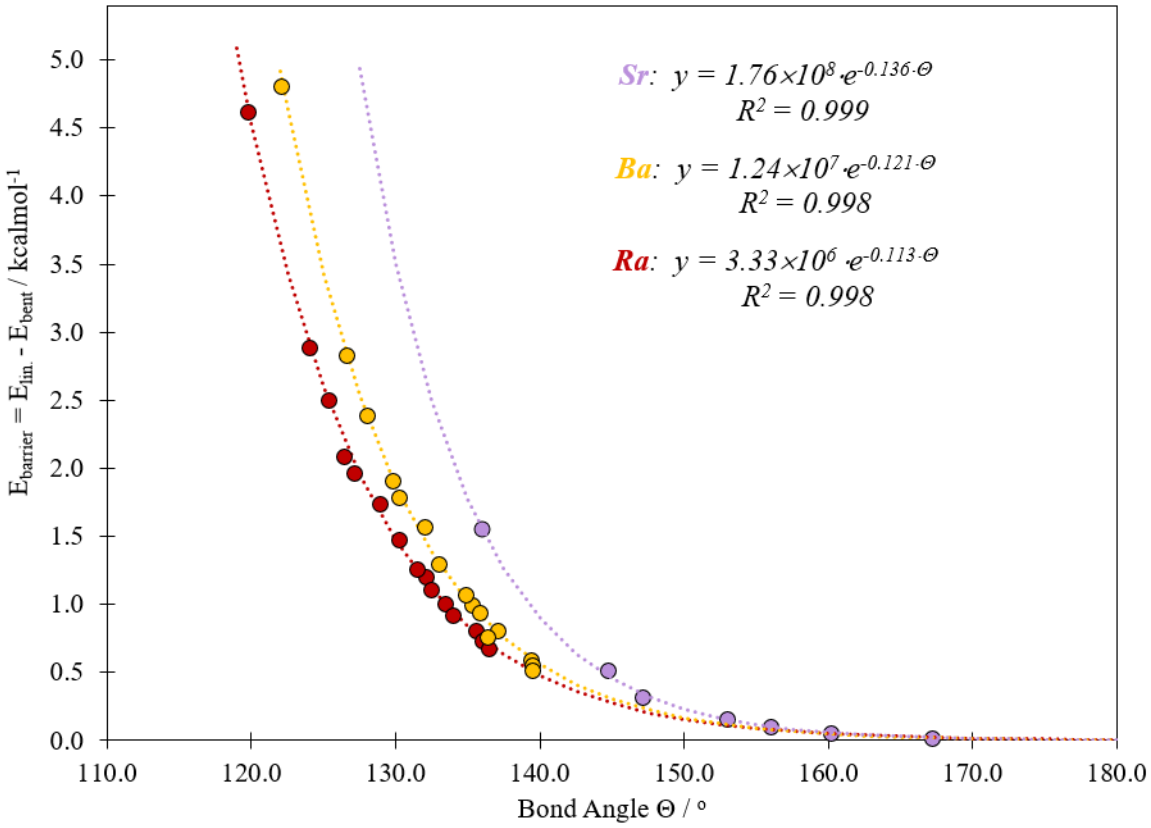

Introduction

The bonding preferences of the symmetric group 2 dihalides (MX_2) are well established: the Be and Mg systems are linear,[1,2,3] and the Ba and Ra systems are bent, as well as SrF_2, $SrCl_2$, and CaF_2.[4,5,6,7,8] The remaining Ca and Sr systems are linear except for few that are described as quasi-linear, i.e. molecules with very flat potential energy surfaces, even if their shallow minimum is bent (CaF_2 and $SrCl_2$)[9,10] or linear ($SrBr_2$).[11]

Since Klemperer *et al.* discovered this phenomenon,[12,13,14] various models have been proposed to account for this bending: electrostatic core-polarization,[15,16,17] an extended VSEPR model,[18,19] and *s*-*d* hybridization on M.[2,4,20,21] Garcia-Fernandez *et al.* went so far as to suggest that the anomalous bending is in fact a manifestation of pseudo Jahn-Teller mixing such that the bent form becomes more stabilized as M gets larger and the halides get smaller and more polarizing.[22] Unfortunately, even though correct trends are yielded if the multipole expansion is not truncated too severely, core-polarization models fail as they predict bond angles that compare poorly with experiment.[10,15,16,17]

(1) Hargittai, M. *Coord. Chem. Rev.* **1988**, *91*, 35−88.
(2) Hargittai, M. *Chem. Rev.* (Washington, DC, U. S.) **2000**, *100*, 2233−2301.
(3) Kaupp, M. *Angew. Chem., Int. Ed.* **2001**, *40*, 3534−3565.
(4) Kaupp, M.; Schleyer, P. v. R.; Stoll, H.; Preuss, H. *J. Am. Chem. Soc.* **1991**, *113*, 6012−6020.
(5) Donald, K. J.; Hoffmann, R. *J. Am. Chem. Soc.* **2006**, *128*, 11236−11249.
(6) Calder, V.; Mann, D. E.; Seshadri, K. S.; Allavena, M.; White, D. *J. Chem. Phys.* **1969**, *51*, 2093−2099.
(7) White, D.; Calder, G. V.; Hemple, S.; Mann, D. E. *J. Chem. Phys.* **1973**, *59*, 6645−6651.
(8) Vasiliu, M.; Hill, J. G.; Peterson, K. A.; Dixon, D. A. *J. Phys. Chem. A* **2018**, *122*, 316−327.
(9) Koput, J.; Roszczak, A. *J. Phys. Chem. A* **2004**, *108*, 9267−9273.
(10) Varga, Z.; Lanza, G.; Minichino, C.; Hargittai, M. *Chem. - Eur. J.* **2006**, *12*, 8345−8357.
(11) Hargittai, M.; Kolonits, M.; Knausz, D.; Hargittai, I. *J. Chem. Phys.* **1992**, *96*, 8980−8985.
(12) Buchler, A.; Klemperer, W. *J. Chem. Phys.* **1958**, *29*, 121−123.
(13) Wharton, L.; Berg, R. A.; Klemperer, W. *J. Chem. Phys.* **1963**, *39*, 2023−2031.
(14) Büchler, A.; Stauffer, J. L.; Klemperer, W. *J. Am. Chem. Soc.* **1964**, *86*, 4544− 4550.
(15) Guido, M.; Gigli, G. *J. Chem. Phys.* **1976**, *65*, 1397−1402.
(16) DeKock, R. L.; Peterson, M. A.; Timmer, L. K.; Baerends, E. J.; Vernooijs, P. *Polyhedron* **1991**, *10*, 1965.
(17) Donald, K. J.; Mulder, W. H.; Szentpaly, L. v. *J. Chem. Phys.* **2003**, *119*, 5423−5436.
(18) Gillespie, R. J. *Molecular Geometry*; van Nostrand Reinhold Company, Ltd.: New York, 1972.
(19) Bytheway, I.; Gillespie, R. J.; Tang, T.-H.; Bader, R. F. W. *Inorg. Chem.* **1995**, *34*, 2407−2414.
(20) Hayes, E. F. *J. Phys. Chem.* **1966**, *70*, 3740−3742.
(21) Kaupp, M.; Schleyer, P.v. R.; Stoll,H.; Preuss, H. *J. Chem. Phys.* **1991**, *94*, 1360−1366.
(22) Garcia-Fernandez, P.; Bersuker, I. B.; Boggs, J. E. *J. Phys. Chem. A* **2007**, *111*, 10409−10415.

Yet Szentpály and Schwerdtfeger have pointed out that core-polarization and orbital mixing are, "two sides of the same coin."[23] In their work, they developed a criterion for the bending of groups 2 and 12 MX_2 and MXY molecules based on atomic softness difference. Atomic softness (σ), is the inverse of atomic hardness, which is defined as the difference between the atomic valence state ionization energy, I_v, and electron affinity, A_v:[23]

$$\sigma = 2\,(I_v - A_v)^{-1}\ eV^{-1} \qquad (1)$$

In their analysis, Szentpály and Schwerdtfeger observed bending when M is large and soft, and X is hard and polarizing enough such that,

$$\Delta\sigma = \sigma_M - \sigma_X > 0.290\ eV^{-1} \qquad (2)$$

For the mixed (ternary) dihalides, they defined σ_{XY} as the arithmetic mean of σ_X and σ_Y, even though there were no known experimental cases of the mixed dihalides at the time.

Surprisingly, the group 12 dihalides are all linear with high bending force constants.[1,24] Their inflexibility has been explained by *d*-orbital and lanthanide contractions as well as relativistic stabilization of the valence *s*-orbitals.[11,23,25,26,27] All three factors serve to reduce atomic softness, disfavoring bending.[11,23] Eventually, Szentpály was able to develop a simple function that was able to partition the groups 2 and 12 dihydrides, dihalides, and dilithides into bent and linear species and to predict the geometries for the MX_2 molecules.[28]

(23) von Szentpály, L.; Schwerdtfeger, P. *Chem. Phys. Lett.* **1990**, *170*, 555−560.
(24) Bratsch, S. G. *J. Chem. Educ.* **1988**, *65*, 34−41.
(25) Donald, K.; Hargittai, M.; Hoffmann, R. *Chem. - Eur. J.* **2009**, *15*, 158−177.
(26) Pyykko, P. *J. Chem. Soc., Faraday Trans. 2* **1979**, *75*, 1256−1276.
(27) Pyykko, P.; Desclaux, J. P. *Acc. Chem. Res*. **1979**, *12*, 276−281.
(28) von Szentpály, L. *J. Phys. Chem. A* **2002**, *106*, 11945-11949.

The bonding in the symmetric groups 2 and 12 dihalides has been extensively studied. Despite Szentpály and Schwerdtfeger's predictions, few isolated investigations on the mixed systems exist.[11,29,30,31,32,33,34] In this work, I carried out a complete assessment of the bonding preferences and vibrational frequencies of the mixed dihalides (MXY) of the groups 2 and 12 metals. A generalized softness criterion is developed for M = Be, Mg, Ca, Sr, Ba, Ra, Zn, Cd, and Hg and X, Y = F, Cl, Br, I and At. For completeness, I include the binary systems as well. A clean separation between the bent and linear structures is achieved. Stretching and bending vibrational frequencies, and force constants are obtained at high levels of theory for the first time for the ternary dihalides of the groups 2 and 12 metals.

Computational Methods

The molecular geometries, harmonic vibrational frequencies, and force constants, for the binary and mixed dihalides considered in this work were obtained at the B3PW91,[35,36] MP2(full) functional,[37] and CCSD(T)[38] computational levels using the Gaussian 09 suite of programs.[39] The frozen core approximation was employed at the CCSD(T) level. In each case, the quintuple zeta (cc-pV5Z) basis sets[40] were employed for

(29) Pyykko, P. *Chem. Rev.* **1988**, *88*, 563−594.
(30) Seth, M.; Dolg, M.; Fulde, P.; Schwerdtfeger, P. *J. Am. Chem. Soc.* **1995**, *117*, 6597−6598.
(31) Strull, A.; Givan, A.; Loewenschuss, A. *J. Mol. Spectrosc.* **1976**, *62*, 283−291.
(32) Givan, A.; Loewenschuss, A. *J. Chem. Phys.* **1976**, *64*, 1967−1972.
(33) Givan, A.; Loewenschuss, A. *J. Mol. Struct.* **1978**, *48*, 325−333.
(34) Givan, A.; Loewenschuss, A. *J. Chem. Phys.* **1980**, *72*, 3809−3821.
(35) Burke, K.; Perdew, J. P.; Wang, Y. Springer: New York, **1998**.
(36) Perdew, J. P.; Burke, K.; Wang, Y. *Phys. Rev. B: Condens. Matter Mater. Phys.* **1996**, *54*, 16533. and references therein.
(37) Head-Gordon, M.; Head-Gordon, T. *Chem. Phys. Lett.* **1994**, *220*, 122−128. and references therein.
(38) Raghavachari, K.; Trucks, G. W.; Pople, J. A.; Head-Gordon, M. *Chem. Phys. Lett.* **1989**, *157*, 479−483.
(39) Frisch, M. J.; Trucks, G. W.; Schlegel, H. B.; Scuseria, G. E.; Robb, M. A.; Cheeseman, J. R.; Scalmani, G.; Barone, V.; Mennucci, B.; Petersson, G. A.; et al. Gaussian 09, Revision D.01; Gaussian, Inc.: Wallingford, CT, 2013.
(40) Peterson, K. A.; Woon, D. E.; Dunning, T. H., Jr. *J. Chem. Phys.* **1994**, *100*, 7410−7415. and references therein.

all elements preceding Br. For heavier elements, the small core MDF pseudopotentials were employed along with the corresponding quintuple zeta basis sets for the higher energy electrons. 10-, 20-, and 25-valence electron effective core MDF pseudopotentials have been deployed, respectively, for the heavy group 2 metals (Sr, Ba, and Ra),[41,42] the group 12 metals (Zn, Cd, and Hg)[43] and the largest halide atoms (Br, I, and At).[44,45] Barriers to linearity ($\Delta E_{barrier} = E_{linear} - E_{minimum}$) have been computed for bent molecules, where E_{linear} is the energy of the linear structure and $E_{minimum}$ is the energy of the minimum energy structure.

Results & Discussion

The structural parameters of the groups 2 and 12 binary (MX_2) and mixed (MXY) dihalides (M = Be, Mg, Ca, Sr, Ba, Ra, Zn, Cd, and Hg and X, Y = F, Cl, Br, I, and At) are shown in Tables 1 and 2. For the mixed systems, X is defined throughout this work as the lighter of the two halides. Furthermore, unless otherwise stated, the data reported has been calculated at the CCSD(T) level of theory.

As seen in Tables 1 and 2, the trend in the computed bond distances reflects the increasing size of the metal and X or Y as you go down groups 2 and 12. Note that the M-X bond lengths progressively shorten as Y gets larger for the group 2 systems, yet the opposite effect is seen for the group 12 systems. This effect can be explained by the difference in shell effects and electronegativities of the groups 2 and 12 metals.

(41) Lim, I. S.; Stoll, H.; Schwerdtfeger, P. *J. Chem. Phys.* **2006**, *124*, 034107.
(42) Peterson, K. A.; Puzzarini, C. *Theor. Chem. Acc.* **2005**, *114*, 283−296.
(43) Figgen, D.; Rauhut, G.; Dolg, M.; Stoll, H. *Chem. Phys.* **2005**, *311*, 227−244.
(44) Peterson, K. A.; Figgen, D.; Goll, E.; Stoll, H.; Dolg, M. *J. Chem. Phys.* **2003**, *119*, 11113−11123.
(45) Peterson, K. A.; Shepler, B. C.; Figgen, D.; Stoll, H. *J. Phys. Chem. A* **2006**, *110*, 13877−13883.

Table 1: Optimized M-X and M-Y bond distances obtained for the Be, Mg, Ca, Sr, Ba, and Ra dihalides.

	M-**X** Bond Distances						M-**Y** Bond Distances					
MXY	Be	Mg	Ca	Sr	Ba	Ra	Be	Mg	Ca	Sr	Ba	Ra
MF_2	1.371	1.714	2.010	2.128	2.236	2.306						
MFCl	1.363	1.718	1.988	2.109	2.212	2.285	1.794	2.100	2.490	2.634	2.773	2.849
MFBr	1.361	1.709	1.983	2.105	2.208	2.281	1.940	2.236	2.638	2.794	2.937	3.014
MFI	1.359	1.712	1.975	2.101	2.201	2.274	2.148	2.433	2.858	3.026	3.175	3.251
MFAt	1.359	1.713	1.975	2.100	2.200	2.273	2.225	2.511	2.929	3.106	3.253	3.328
MCl_2	1.784	2.088	2.463	2.613	2.745	2.824						
MClBr	1.782	2.082	2.457	2.610	2.738	2.818	1.930	2.231	2.610	2.775	2.907	2.989
MClI	1.780	2.075	2.451	2.603	2.732	2.812	2.139	2.411	2.828	3.004	3.144	3.227
MClAt	1.780	2.075	2.450	2.600	2.731	2.810	2.215	2.485	2.903	3.082	3.222	3.303
MBr_2	1.927	2.228	2.658	2.858	2.903	2.983						
MBrI	1.926	2.229	2.600	2.760	2.895	2.977	2.137	2.420	2.825	2.998	3.140	3.221
MBrAt	1.926	2.232	2.599	2.759	2.893	2.977	2.216	2.499	2.900	3.074	3.215	3.300
MI_2	2.136	2.417	2.819	2.988	3.132	3.215						
MIAt	2.136	2.419	2.817	2.986	3.131	3.214	2.215	2.495	2.890	3.065	3.206	3.291
MAt_2	2.214	2.499	2.889	3.133	3.206	3.290						

Table 2: Optimized M-X and M-Y bond distances obtained for the Zn, Cd, and Hg dihalides.

	M-**X** Bond Distances			M-**Y** Bond Distances		
MXY	Zn	Cd	Hg	Zn	Cd	Hg
MF_2	1.714	1.916	1.910			
MFCl	1.721	1.923	1.928	2.053	2.249	2.226
MFBr	1.724	1.926	1.935	2.180	2.368	2.346
MFI	1.727	1.930	1.947	2.362	2.539	2.515
MFAt	1.730	1.933	1.954	2.435	2.607	2.585
MCl_2	2.062	2.258	2.247			
MClBr	2.067	2.263	2.257	2.189	2.378	2.368
MClI	2.071	2.270	2.267	2.373	2.551	2.536
MClAt	2.074	2.272	2.275	2.444	2.616	2.603
MBr_2	2.192	2.382	2.375			
MBrI	2.197	2.389	2.387	2.379	2.556	2.542
MBrAt	2.201	2.392	2.394	2.450	2.622	2.611
MI_2	2.382	2.562	2.554			
MIAt	2.387	2.598	2.593	2.456	2.598	2.593
MAt_2	2.457	2.632	2.628			

Table 3 and Figure 1 show the computed bond angles and up-to-date experimental electron diffraction values.[9,44,46,47,48,49] Although of active interest,[50,51,52,53,54] investigations into the mixed systems are sparse, save for few spectroscopic studies.[55,56] Unfortunately, no experimental geometries were found for the mixed systems.

Table 3: Optimized MXY bond angles for the Ca, Sr, Ba, and Ra dihalides. For M = Be, Mg, Zn, Cd and Hg the structures were found to be linear (Θ = 180.0º). Experimental electron diffraction values are shown in brackets.

	Computed Bond Angles			
MXY	Ca	Sr	Ba	Ra
MF_2	158.0	136.0	122.2	119.9
MFCl	180.0	144.8	126.7	124.1
MFBr	180.0	147.3	128.1	125.5
MFI	180.0	153.1	129.9	126.5
MFAt	180.0	156.1	130.3	127.2
MCl_2	180.0 (lin)	160.3 (154.6)	132.1	129.0
MClBr	180.0	167.3	133.1	130.4
MClI	180.0	180.0	135.4	132.2
MClAt	180.0	180.0	135.9	132.6
MBr_2	180.0 (lin)	180.0 (q.lin.)	135.0 (137.0)	131.6
MBrI	180.0	180.0	137.2	133.6
MBrAt	180.0	180.0	136.5	134.1
MI_2	180.0 (lin)	180.0 (180.0)	139.5 (137.6)	135.7
MIAt	180.0	180.0	139.6	136.2
MAt_2	180.0	180.0	139.6	136.6

Across all three methods, the Be and Mg systems as well as those of the group 12 are predicted to be linear, i.e. the X-M-Y bond angle, Θ, is 180º. As can be seen in Table 3 and Figure 1, going down the series, the molecules eventually begin to bend as M gets

(46) Kasparov, V. V.; Ezhov, Y. S.; Rambidi, N. G. *J. Struct. Chem.* **1979**, *20*(2), 285−288.
(47) Spiridonov, V. P.; Gershikov, A. G.; Altman, A. B.; Romanov, G. V.; Ivanov, A. *Chem. Phys. Lett.* **1981**, *77*, 41−44.
(48) Vajda, E.; Hargittai, M.; Hargittai, I.; Tremmel, J.; Brunvoll, J. E*Inorg. Chem.* **1987**, *26*, 1171−1174.
(49) Hargittai, M.; Kolonits, M.; Schultz, G. *J. Mol. Struct.* **2001**, *567-568*, 241−246.
(50) Beck, H. P. *Z. Anorg. Allg. Chem.* **1979**, *459*,72−80.
(51) Scott, J. F. *J. Chem. Phys.* **1968**, *49*, 2766−2769.
(52) Bhat, T. N.; Bhat, H. L.; Rao, A. H.; Srinivasan, M. R.; Narayanan, P. S. *Curr. Sci.* **1978**, *47*, 204−206.
(53) Beck, H. P. *Z. Anorg. Allg. Chem.* **1979**, *451*, 73−81.
(54) Haeuseler, H. *Phys. Chem. Miner.* **1981**, *7*, 135−137.
(55) Givan, A.; Loewenschuss, A. *J. Chem. Phys.* **1978**, *68*, 2228−2242.
(56) Givan, A.; Loewenschuss, A. *Spect. Acta A: Mol. Spect.* **1978**, *34*, 765−770.

larger and as X and Y become more polarizing, lending some amount of credence to the pseudo Jahn-Teller mixing as suggested by Garcia-Fernandez *et al.*[22] In the case of the binary dihalides, Θ gets smaller as M gets larger - RaF_2 is computed to be the most bent (119.9º) and CaF_2 is predicted to be the least bent (158.0º). As seen in Figure 1, holding M constant, Θ increases as X and Y get heavier, however, this increase isn't always uniform, see BaBrI and BaBrAt. BaBrI is predicted to be slightly more bent than BaBrAt and although this astatine/iodine inversion is even more prominent at the MP2(full) level, it is absent at the B3PW91 level. We surmise that this I/At inversion is driven primarily by electron correlation, exaggerated at the MP2(full) level but inadequately accounted for at the B3PW91 level.

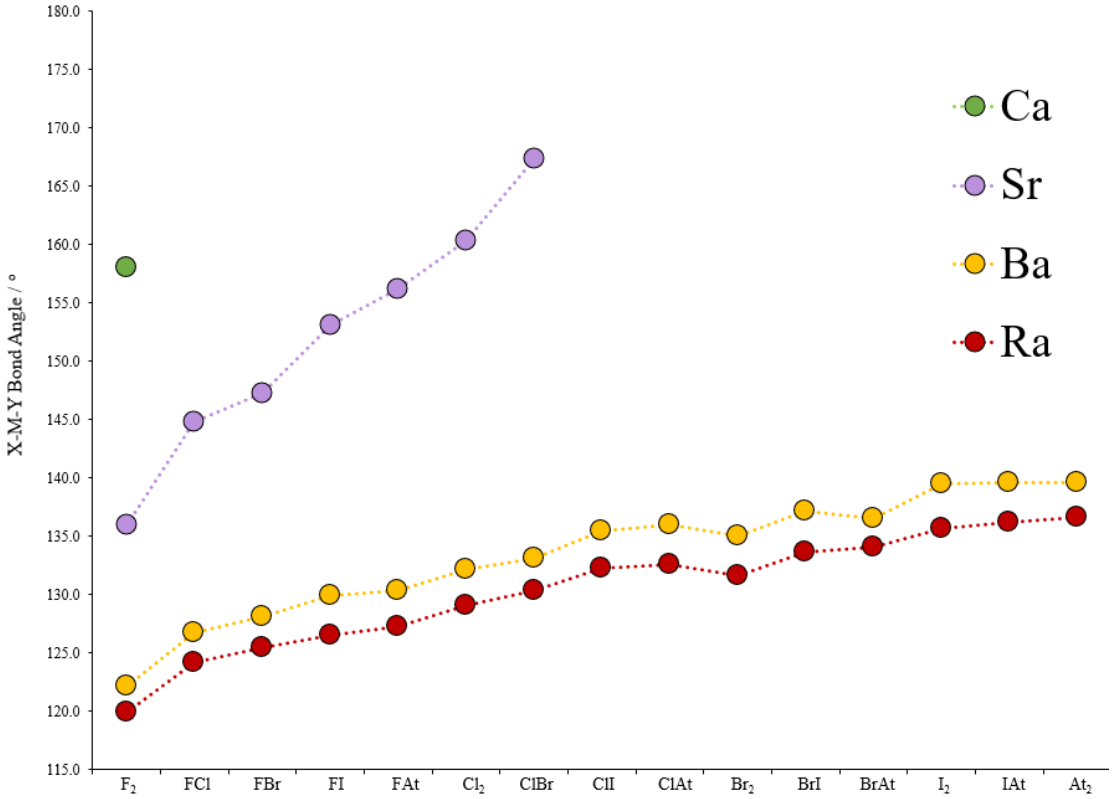

Figure 1: Graph of the computed bond angles for the bent M = Ca, Sr, Ba and Ra cases. Systems not shown were computed to be linear.

Fortunately, the B3PW91 data otherwise align well qualitatively with the values obtained at the *ab initio* levels, however for the floppy SrXY and CaFY molecules, the computed values no longer agree. For example, CaFCl and CaFBr are predicted to be bent at the B3PW91 level of theory yet both systems were predicted to be linear at both *ab initio* levels. A comparison between our current B3PW91 values and previous B3LYP data for the binary dihalides[6] show good agreement, leading us to conclude that popular DFT methods appear to perform poorly for the metal dihalides if the surfaces are particularly flat. However, our assumption that DFT methods perform poorly is predicated on the idea that our *ab initio* methods, are in fact, correct. We are comfortable making this assumption because the electron diffraction data available show good agreement with our values calculated at the *ab initio* levels, as seen in Table 3.

A direct investigation of this I/At inversion is yet to be confirmed, especially considering that the I/At inversion is only seen in the BaXY series. Additionally, the differences in the general trend in the M-X distance as Y gets larger for group 2 vs. the group 12 mixed dihalides provides an additional route for experimental investigation.

Previously established trends of the binary dihalides (with Θ decreasing as M gets larger and X gets smaller) allow us to predict that RaF_2 would be the most bent system. Our predicted value of 119.9° is in line with Lee *et al.*'s predicted bond angle of 118°.[57] Our results show that while a linear geometry is the maximum X-M-Y angle achieved, RaF_2's is the lower bound across all systems, binary or ternary.

(57) Lee, E. P. F.; Soldán, P.; Wright, T. G. *Inorg. Chem.* **2001**, *40*, 5979−5984.

Barriers to Linearization. We show in Figure 2 the magnitudes of the barriers to linearization (without zero-point corrections) for the bent molecules. Molecules found to have low barriers to linearization can be described as floppy, meaning that experimental distances may differ from the computed bond distances.[58] In some cases, the geometry of these floppy systems are ambiguous due to the nature (and magnitude) of the interactions in matrix isolation studies.[54,55]

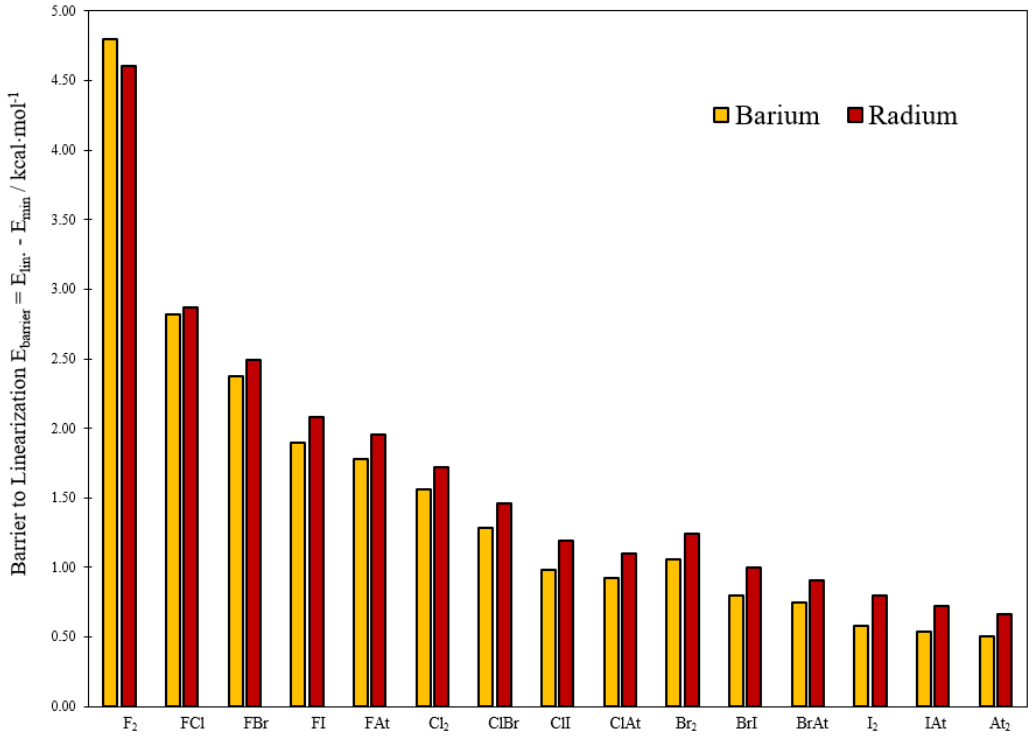

Figure 2: Barriers to linearization at the CCSD(T) level for the Ba and Ra dihalides. For the Sr and Ca systems that are bent the well depths in kcalmol^{-1} units are as follows: for SrFY: 1.54, 0.50, 0.31, 0.15, and 0.09, for Y = F, Cl, Br, I, and At, with 0.04 for $SrCl_2$, and 0.00 to two decimal places for SrClBr. For CaF_2, and CaFCl we obtained a barrier of 0.07 and 0.00 kcalmol^{-1} respectively.

The most surprising takeaway from Figure 2 is that RaF_2 is predicted to have a barrier to linearization slightly smaller than that of BaF_2, although the former is predicted

(58) Hargittai, M.; Hargittai, I. *Int. J. Quantum Chem.* **1992**, *44*, 1057−1067.

to be more bent. Fortunately, this is the only system we find to have a shallower potential well than expected. Moreover, the difference in the two is small enough to be considered insignificant (0.19 $kcalmol^{-1}$). This insignificance holds true when the linearization free energies are calculated (0.27 $kcalmol^{-1}$). Although this offers another opportunity for experimentalists, we anticipate practical difficulties with radium compounds which would make it difficult to further clarify these results.

A fair assumption to make at this point is that very bent systems will possess larger barriers to linearization, i.e. that the barrier to linearization is directly proportional to bond angle. This assumption is challenged by the barrier of RaF_2 compared to BaF_2. Therefore, to elucidate this relationship, we graph the two against one another, as shown in Figure 3 below. The data we obtain may be fitted – with coefficients of determination in excess of 0.995 at the CCSD(T) level – with the form:

$$E_{barrier}(\Theta) \equiv y = Ae^{-k\Theta} \qquad (3)$$

where A is the energy barrier for a hypothetical system with a minimum bond angle $\Theta = 0$ and k is a constant with units of $degrees^{-1}$. It is comforting to find that the fitted graphs approach zero as the bond angle approached 180^{o} which, when combined with the high coefficients of determination, suggest a definite relationship between the energy barriers and bond angle for a given M.

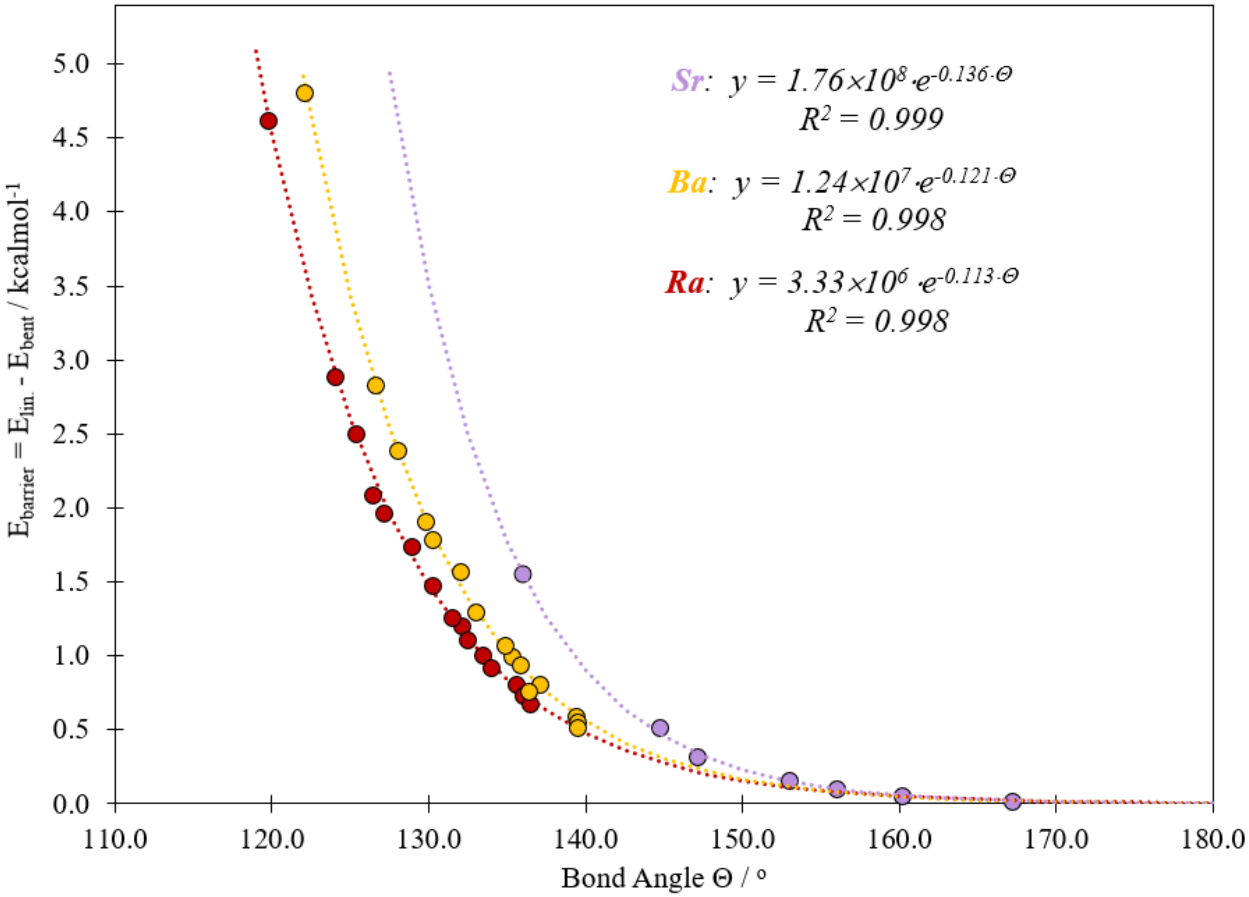

Figure 3: A representation of the relationship between bond angle and the energy barriers to linearization, $E_{barrier}$, for the bent group 2 binary and ternary dihalides of Sr, Ba, and Ra.

Bending and the Softness Criterion. While the equations from Figure 3 allow us to predict the energy barriers for bent systems, we are not yet able to predict which systems will be bent. Fortunately, the data we have gathered allow us to develop an extension of the softness criterion proposed by Szentpály and Schwerdtfeger based on the softness difference between the central atom (M) and the halogen atoms (X and Y) in the molecule.[23]

Table 4: Atomic softnesses, σ, in eV^{-1} units.

M	σ	M	σ	X/Y	σ
Be	0.304	Ra	0.543	F	0.114
Mg	0.380	Zn	0.338	Cl	0.175
Ca	0.446	Cd	0.338	Br	0.196
Sr	0.480	Hg	0.344	I	0.216
Ba	0.509			At	0.20

Szentpály and Schwerdtfeger's criterion was based on valence state atomic softness (as shown in (2)) and succeeded in separating the bent and linear binary dihalides that they considered (with $\Delta\sigma > 0.290$ eV^{-1} for bent structures). Additionally, they suggested a criterion for the mixed dihalides, using the arithmetic mean ($\sigma_{XY} = \frac{\sigma_X + \sigma_Y}{2}$) of X and Y. Using the softness values shown in Table 4, we have computed softness differences for the mixed dihalides using Szentpály and Schwerdtfeger's criterion, shown in Table 5 below.

Szentpály and Schwerdtfeger's proposed softness criterion, using the arithmetic mean, achieves an almost perfect separation of the bent and linear mixed groups 2 and 12 dihalides. We find that the best partition is achieved with a threshold of 0.292 eV^{-1}, such that when $\Delta\sigma > 0.292$ eV^{-1}, the system is predicted to be bent.

We propose an alternative criterion, one using the weighted mean of the halides:

$$\sigma_{XY} = w_X\sigma_X + {}_Y\sigma_Y \qquad (4)$$

where the weighting factors are $w_X = \frac{\sigma_X}{\sigma_X + \sigma_Y}$ and $w_Y = \frac{\sigma_Y}{\sigma_X + \sigma_Y}$, such that the weighted mean reliably reflects the contributions of the relative softness to the average. Again, using the softness values shown in Table 4, we have computed softness differences for the mixed dihalides using our proposed criterion, shown in Table 6 below.

Table 5: Softness differences, Δσ, and basic geometries for MXY molecules, where Δσ is the difference between σ_M and the arithmetic mean of σ_X and σ_Y. Pink and white cells indicate systems with bent and linear geometries respectively. Green cells indicate systems with linear geometries but predicted to be bent using Szentpály and Schwerdtfeger's softness criterion.

MXY	Be	Mg	Ca	Sr	Ba	Ra	Zn	Cd	Hg
MF_2	0.190	0.266	0.332	0.366	0.395	0.429	0.224	0.224	0.230
MFCl	0.160	0.236	0.302	0.336	0.365	0.399	0.194	0.194	0.200
MFBr	0.149	0.225	0.291	0.325	0.354	0.388	0.183	0.183	0.189
MFI	0.139	0.215	0.281	0.315	0.344	0.378	0.173	0.173	0.179
MFAt	0.147	0.223	0.289	0.323	0.352	0.386	0.181	0.181	0.187
MCl_2	0.129	0.205	0.271	0.305	0.334	0.368	0.163	0.163	0.169
MClBr	0.119	0.195	0.261	0.295	0.324	0.358	0.153	0.153	0.159
MClI	0.109	0.185	0.251	0.285	0.314	0.348	0.143	0.143	0.149
MClAt	0.117	0.193	0.259	*0.293	0.322	0.356	0.151	0.151	0.157
MBr_2	0.108	0.184	0.250	0.284	0.313	0.347	0.142	0.142	0.148
MBrI	0.098	0.174	0.240	0.274	0.303	0.337	0.132	0.132	0.138
MBrAt	0.106	0.182	0.248	0.282	0.311	0.345	0.140	0.140	0.146
MI_2	0.088	0.164	0.230	0.264	0.293	0.327	0.122	0.122	0.128
MIAt	0.096	0.172	0.238	0.272	0.301	0.335	0.130	0.130	0.136
MAt_2	0.104	0.180	0.246	0.280	0.309	0.343	0.138	0.138	0.144

Table 6: Softness differences, Δσ, and basic geometries as obtained for MXY molecules, where Δσ is the difference between σ_M and a weighted average of σ_X and σ_Y. Pink and white cells indicate systems with bent and linear geometries respectively. Green cells indicate systems with linear geometries but predicted to be bent using our softness criterion.

MXY	Be	Mg	Ca	Sr	Ba	Ra	Zn	Cd	Hg
MF_2	0.190	0.266	0.332	0.366	0.395	0.429	0.224	0.224	0.230
MFCl	0.153	0.229	0.295	0.329	0.358	0.392	0.187	0.187	0.193
MFBr	0.138	0.214	0.280	0.314	0.343	0.377	0.172	0.172	0.178
MFI	0.123	0.199	0.265	0.299	0.328	0.362	0.157	0.157	0.163
MFAt	0.135	0.211	0.277	0.311	0.340	0.374	0.169	0.169	0.175
MCl_2	0.129	0.205	0.271	0.305	0.334	0.368	0.163	0.163	0.169
MClBr	0.118	0.194	0.260	0.294	0.323	0.357	0.152	0.152	0.158
MClI	0.106	0.182	0.248	0.282	0.311	0.345	0.140	0.140	0.146
MClAt	0.116	0.192	0.258	0.292	0.321	0.355	0.150	0.150	0.156
MBr_2	0.108	0.184	0.250	0.284	0.313	0.347	0.142	0.142	0.148
MBrI	0.098	0.174	0.240	0.274	0.303	0.337	0.132	0.132	0.138
MBrAt	0.106	0.182	0.248	0.282	0.311	0.345	0.140	0.140	0.146
MI_2	0.088	0.164	0.230	0.264	0.293	0.327	0.122	0.122	0.128
MIAt	0.096	0.172	0.238	0.272	0.301	0.335	0.130	0.130	0.136
MAt_2	0.104	0.180	0.246	0.280	0.309	0.343	0.138	0.138	0.144

As seen in Table 6, a much cleaner separation is achieved using the weighted average instead of the arithmetic. It is especially comforting to note that the criterion is the same in both cases ($\Delta\sigma > 0.292$ eV^{-1}).

We find certain molecules that are predicted to be linear possess a $\Delta\sigma$ value that is just at or above the bending cutoff. Fortunately, there are only two: CaFCl using both criteria and SrClAt using Szentpály and Schwerdtfeger's criterion. For both systems, their potential energy surfaces are extremely flat, with barriers of 0.00 $kcalmol^{-1}$. Without a rigorous quantum mechanical definition of quasi-linearity, it is difficult to identify which molecules can be classified as such. Kaupp chose to use an energy cutoff with quasi-linear molecules having a maximum energy change of ~ 4 $kJmol^{-1}$ (~ 1 $kcalmol^{-1}$) for a deviation greater than 20° from linearity.[3] However, if we take into account that $SrCl_2$ and $SrBr_2$ are wholly accepted to be bent and quasi-linear respectively, we can use them as our references. We are then able to make the claim that systems with $\Delta\sigma$ values between or close to those of $SrCl_2$ and $SrBr_2$ can therefore be considered quasi-linear.

Conclusion

Very little is known about the bonding of group 2 ternary dihalides in the gas phase. Structural investigations are sparse and isolated even though it is well-known that many of the group 2 binary dihalides are bent in the gas phase. In this work, I have investigated structural preferences of the mixed cases – as well as the groups 2 and 12 binary dihalides, for M = Be, Mg, Ca, Sr, Ba, and Ra, with X and Y = F, Cl, Br, I, and At. I find that the trend observed for the binary dihalides are like that observed of the ternary systems, except for BaBrAt and BaBrI. Additionally, I find that the barriers to linearization for the group 2

dihalides are defined by the function $E_{barrier}(\Theta) = Ae^{-k\Theta}$, where Θ is the bond angle, and A and k are constants, specific to a given metal but are found to hold for all the halides considered.

The *ab initio* methods show good quantitative agreement on the geometrical properties of the molecules. B3PW91 tends to predict smaller bond angles for bent systems and more bent minimum energy geometries in the series of group 2 mixed dihalides compared to the *ab initio* methods. We await experimental resolutions to this disagreement, especially for the floppiest molecules. Electron diffraction data may be able to supply definitive experimental insights into the nature of these systems.

Chapter 2

Competing Channels for the Bonding of Borylene Complexes

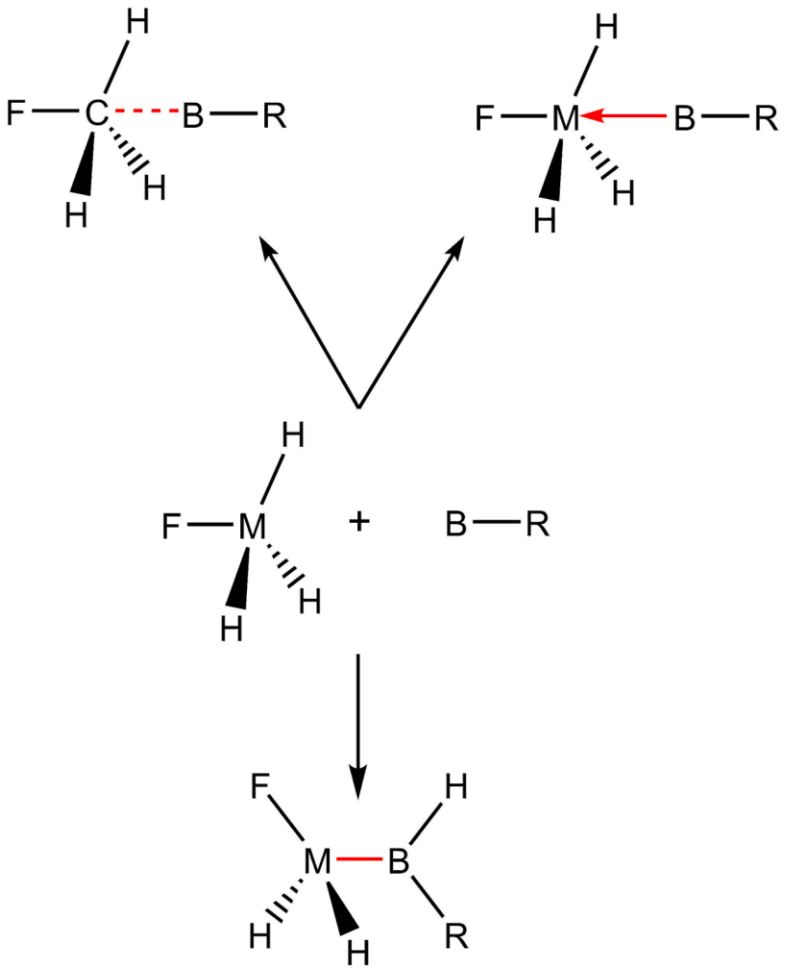

Abstract

Only isolated or case specific pieces of experimental information are available to date for free monovalent boron and borylene compounds. A systematic investigation is missing from the literature so there are substantial gaps in our understanding of borylenes and their possible utility in organic and inorganic chemistry - either as ligands or intermediates in complex chemical reactions. In this work, I show that the relative stability of borylene complexes varies widely, depending on the electron donating ability of the R groups (considering a diverse range of R substituents). I find strong enough attractive interactions between several B-R and MH_3F Lewis acids (where M = C, Si, and Ge) such that the $R'H_3M$---BR→ $R'H_2M$-BHR reaction is barrierless in some cases. In fact, for Si, a barrier only appears when R is a very strong electron withdrawing group. For Ge, the reaction is barrierless only in cases where R is a very large, electron donating group. In contrast, the barriers are very high for C across all R substituents.

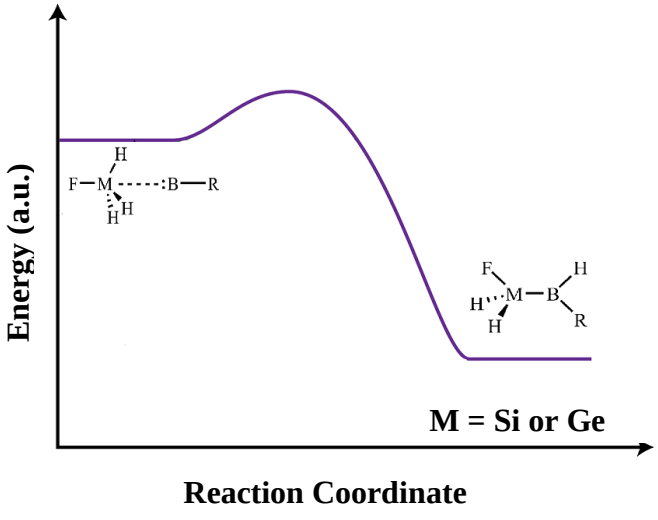

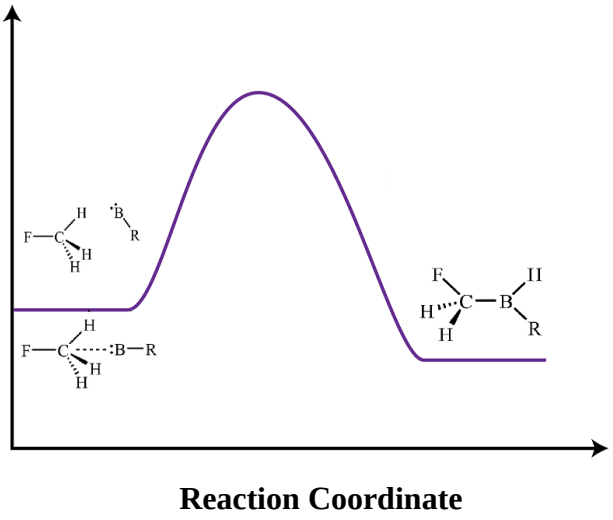

Introduction

When we think of electron donors in the second row of the periodic table, nitrogen and oxygen most easily come to mind. :NR_3 and :$\ddot{O}R_2$ compounds, such as ammonia (NH_3) and water (OH_2), stereotypically react with Lewis acids to form simple compounds. It is easy to see why they have become the go-to Lewis bases: they are both electron donating, typically inexpensive and computationally less demanding than their heavier (e.g. P and S) analogues. They are also stable under a wide range of chemical and thermodynamic conditions. Unfortunately, other second row bases, specifically carbenes (:CR_2) and borylenes (:BR), are not and the stabilization and utility of these compounds remain active areas of research.

Yet, carbene and borylene chemistry are at very different places in their development: carbenes have been synthesized and studied since the 1990s,[1] but very few isolated pieces of experimental information are available for borylene compounds. Boron monofluoride (BF), for example, is isoelectronic with CO and N_2, but BF and other free BR species that have been detected experimentally are very reactive and are impractical in reactions at ambient conditions.[2,3,4,5,6,7,8,9] A systematic theoretical investigation is missing from the literature so there are substantial gaps in our understanding of borylenes and their possible utility in organic and inorganic chemistry – either as ligands or intermediates in

(1) Arduengo, A. J.; Harlow, R. L.; Kline, M. *J. Am. Chem. Soc.* **1991**, *113*, 361−363.
(2) Blauer, J.; Greenbaum, M. A.; Farber, M. *J. Phys. Chem.* **1964**, *68*, 2332− 2334.
(3) Timms, P. L. *J. Am. Chem. Soc.* **1967**, *89*, 1629−1632.
(4) Timms, P. L. *J. Am. Chem. Soc.* **1968**, *90*, 4585− 4589.
(5) Hildenbrand, D. L.; Murad, E. *J. Chem. Phys.* **1965**, *43*, 1400−1403.
(6) Lovas, F. J.; Johnson, D. R. *J. Chem. Phys.* **1971**, *55*,41−44.
(7) Pianalto, F. S.; O'Brien, L. C.; Keller, P. C.; Bernath, P. F. *J. Mol. Spectrosc.* **1988**, *129*, 348−353.
(8) Bettinger, H. F. *J. Am. Chem. Soc.* **2006**, *128*, 2534−2535.
(9) Braunschweig, H.; Dewhurst, R. D.; Gessner, V. H. *Chem. Soc. Rev.* **2013**, *42*, 3197−3208.

complex chemical reactions. To be clear, borylenes have proven difficult to isolate but its units have been identified before: in matrix isolation studies and trapping reactions.[8,10,11,12,13,14,15] Fortunately, the literature on monovalent boron is growing despite its difficult synthesis.[9,16] Indeed, efforts have been made to locate free borylenes (BR),[15] terminal borylene (Q←BR)[17] and metal-borylene complexes (M=BR).[9,16] In fact, a borylene dicarbonyl complex was reported recently,[18] reiterating borylenes' ability to serve as Lewis acids and act as "metallomimics".[16] Separately, borylenes are stabilized by donors, such as heterocyclic carbenes.[15,19] Insertion of borylene units into C-H and C-C bonds and cycloaddition have been investigated computationally and experimentally.[4,10,12,20,21,22,23] In those reactions, the boron acted as both acceptor (due to its empty p-orbitals) and σ-donor (due to its lone pair).

Previously, our research group has investigated sigma (σ) hole interactions.[24,25,26] A σ-hole can be described as a localized region of positive electrostatic potential induced on an atom, A, by a strongly electron withdrawing substituent, E.[26,27] In a σ-hole interaction, an electron-rich site on a base, such as :N on :NH_3, aligns with the σ-hole on a polarized

(10) Andrews, L.; Hassanzadeh, P.; Martin, J. M. L.; Taylor, P. R. *J. Phys. Chem.* **1993**, *97*, 5839−5847.
(11) Thompson, C. A.; Andrews, L.; Martin, J. M. L.; El-Yazal, J. *J. Phys. Chem.* **1995**, *99*, 13839−13849.
(12) Pachaly, B.; West, R. *Angew. Chem., Int. Ed. Engl.* **1984**, *23*, 454−455.
(13) Ito, M.; Tokitoh, N.; Kawashima, T.; Okazaki, R. *Tetrahedron Lett.* **1999**, *40*, 5557−5560.
(14) Bissinger, P.; Braunschweig, H.; Kraft, K.; Kupfer, T. *Angew. Chem., Int. Ed.* **2011**, *50*, 4704− 4707.
(15) Curran, D. P.; Boussonnière, A.; Geib, S. J.; Lacôte, E. *Angew. Chem., Int. Ed*. **2012**, *51*, 1602−1605.
(16) Bertrand, G.; Soleilhavoup, M. *Angew. Chem., Int. Ed*. **2017**, *56*, 10282−10292.
(17) Cowley, A. H.; Lomelí, V.; Voigt, A. *J. Am. Chem. Soc.* **1998**, *120*, 6401−6402.
(18) Braunschweig, H.; Dewhurst, R. D.; Hupp, F.; Nutz, M.; Radacki, K.; Tate, C. W.; Vargas, A.; Ye, Q. *Nature* **2015**, *522*, 327−330.
(19) Kinjo, R.; Donnadieu, B.; Celik, M. A.; Frenking, G.; Bertrand, G. *Science* **2011**, *333*, 610−613
(20) Meller, A. *Pure Appl. Chem.* **1991**, *63*, 395−398.
(21) Grigsby, W. J.; Power, P. P. *J. Am. Chem. Soc.* **1996**, *118*, 7981−7988.
(22) Krasowska, M.; Bettinger, H. F. *J. Am. Chem. Soc.* **2012**, *134*, 17094− 17103.
(23) Krasowska, M.; Bettinger, H. F. *Chem. - Eur. J.* **2014**, *20*, 12858−12863.
(24) Donald, K. J.; Wittmaack, B. K.; Crigger, C. *J. Phys. Chem. A* **2010**, *114*, 7213−7222.
(25) Tawfik, M.; Donald, K.J. *J. Phys. Chem. A* **2014**, *118*, 10090−10100.
(26) Donald, K. J.; Tawfik, M. *J. Phys. Chem. A* **2013**, *117*, 14176−14183.
(27) Politzer, P.; Murray, J.S.; Lane, P.; Concha,M.C. *Int. J. Quantum Chem.* **2009**, *109*, 3773−3780.

atomic center, A, to form a weakly bound complex, i.e. E−A---Base. Although these electrostatic interactions tend to be weak, charge transfer to the available and appropriate orbitals on A can follow, such that the overall pair is a coordinate covalent, or "*dative*", E−A←Base interaction. Halogen bonding (e.g., Cl−I---:NH_3, where E = Cl and A = I) is one such example. Additionally, the location of the sigma hole on A causes σ-hole interactions to favor linear E−M−Base bond angles.[28] We have shown that the availability of the lone pair on the base (hence the strength of the A−Base bond) is very sensitive to the identity of the substituents on the base.[26,29] In the case of F_4M←:NR_3 pairs for M = Si and Ge, for instance, the identity of R is instrumental for the binding energies and the lengths of the M---N interactions. In the cases where the base is a free borylene species, BR, I find herein that the identity of the substituent, R, plays a key role in determining the nucleophilicity of the base. The electron donating power of R controls the stability of the base and determines whether BR forms a stable acid←base pair as a local minimum or activates the M−H bond instead and forms an insertion product with a trivalent boron center.

The substituent dependence of the reactivity of free borylenes, gas phase or otherwise, has not been systematically examined experimentally. That is certainly because of the instability of borylenes, but the evidence that is available for :CR_2 and :NR_3 species suggests that strategically selected substituents can confer a substantial degree of stability upon the lone pairs of simple bases. Hence, our decision to assess the sensitivity of

(28) Wilcken, R.; Zimmermann, M. O.; Lange, A.; Joerger, A. C.; Boeckler, F. M. *J. Med. Chem.* **2013**, *56*, 1363−1388.
(29) Donald, K. J.; Tawfik, M.; Buncher, B. *J. Phys. Chem. A* **2015**, *119*, 3780−3788.

borylenes in that regard for substituents, R, with very different abilities as electron donating and withdrawing groups. Unlike carbenes, where the triplet state is preferred, the borylenes that have been studied to date are more stable as singlets,[30] and general strategies for stabilizing or engaging them as σ-donors or -acceptors are being developed.[9,16,31] The implications of our results for progress in group 14 chemistry are discussed. My work is situated within the context of efforts in our group to understand the influence of sigma hole interactions on coordinate covalent bonding to group 14 compounds. Especially for M = Si, we find that the progress from dative $FH_3M{\leftarrow}BR$ interactions to BR insertion to form $FH_2M{-}BHR$ may be fully suppressed or promoted depending on the identity of the substituents, R, on the monovalent boron center.

Computational Methods

The geometrical, harmonic vibrational frequency, and internal reaction coordinate (IRC) data reported in this work have been obtained at the MP2(full) level of theory[32] using the Gaussian 09 (G09) suite of programs,[33] with some additional calculations carried out at the B3LYP[34,35] level in tandem with the D3 dispersion correction[36] and at the CCSD(T)[37] level as well. In each case, the correlation-consistent triple-ζ (cc-pVTZ) basis sets were employed for elements above iodine in the periodic table.[38] A small (28-electron) core multielectron Dirac−Fock (MDF) relativistic effective core potential (without the spin−

(30) Krasowska, M.; Edelmann, M.; Bettinger, H. F. *J. Phys. Chem. A* **2016**, *120*, 6332−6341.
(31) Vidovic, D.; Aldridge, S. *Angew. Chem., Int. Ed.* **2009**, *48*, 3669−3672.
(32) Head-Gordon, M.; Head-Gordon, T. *Chem. Phys. Lett.* **1994**, *220*, 122−128 and references therein.
(33) Frisch, M. J.; Trucks, G. W.; Schlegel, H. B.; Scuseria, G. E.; Robb, M. A.; Cheeseman, J. R.; Scalmani, G.; Barone, V.; Mennucci, B.; Petersson, G. A.; et al. Gaussian 09, Revision D.01; Gaussian, Inc.: Wallingford, CT, 2013.
(34) Becke, A. D. *J. Chem. Phys.* **1993**, *98*, 5648−5652.
(35) Stephens, P. J.; Devlin, F. J.; Chabalowski, C. F.; Frisch, M. J. *J. Phys. Chem.* **1994**, *98*, 11623−11627.
(36) Grimme, S.; Antony, J.; Ehrlich, S.; Krieg, H. *J. Chem. Phys.* **2010**, *132*, 154104.
(37) Raghavachari, K.; Trucks, G. W.; Pople, J. A.; Head-Gordon, M. *Chem. Phys. Lett.* **1989**, *157*, 479−483.
(38) Dunning, T. H. *J. Chem. Phys.* **1989**, *90*, 1007−1023.

orbit part) and the corresponding cc-pVTZ basis set[39] for valence electrons were employed for iodine. All of the molecular representations and images included in this article have been generated using the Gaussview graphical user interface[40] and the Chemcraft program.[41] The Synchronous Transit-guided Quasi-Newton−Raphson method as implemented in the Gaussian 09 software (i.e., the QST2 and QST3 options, the latter requiring a guess transition state (TS) structure) was employed to elucidate the nature of the potential energy surface (PES). In particular, the QSTn calculations aided us in our search for credible candidate transition state structures that link weakly bound or dative $FH_3M{\leftarrow}BR$ pairs and insertion products. The scan option was employed to elucidate the nature of the potential energy surface (PES) between local minima as well. Structures obtained from the QSTn or scan data were reoptimized (as transition states) and confirmed by vibrational frequency calculations to be first order saddle points. A refined picture of each insertion reaction was achieved finally by calculating IRC paths using the confirmed TS structures. The number of IRC data points was effectively unrestricted; high "maxpoints" values were used so that the IRC terminated before any limit on the number of points was reached. The counterpoise correction[42,43] as implemented in the G09 suite was used to correct for basis set superposition errors (BSSEs) in computed binding energies for the $FH_3M{\leftarrow}BR$ pair interactions. The Wiberg bond indices and other population

(39) Peterson, K.; Shepler, B.; Figgen, D.; Stoll, H. *J. Phys. Chem. A* **2006**, *110*, 13877−13883.
(40) Dennington, R.; Keith, T.; Millam, J. GaussView, Version 5; Semichem Inc.: Shawnee Mission, KS, 2009.
(41) Chemcraft: Andrienko, A. G.; Senchenya, I. N.; Romanov, A.; http://www.chemcraftprog.com.
(42) Boys, S. F.; Bernardi, F. *Mol. Phys.* **1970**, *19*, 553−566.
(43) For a description of this procedure, see: Jensen, F. Introduction to Computational Chemistry; Wiley: New York, 1999; pp 172−173.

analysis data that we report herein have been obtained from natural bond orbital (NBO) analyses on optimized geometries.

Results & Discussion

The stability of borylene complexes of the form $FH_3M{\leftarrow}{:}BR$ has been examined for M = C, Si, and Ge, and R = H, F, Cl, Br, I, CN, CH_3, $CH_3C{=}CH_2$, $CH_{3-n}(CH_3)_n$ (for n = 1, 2, and 3), and $C(CH_3)_{3-n}(C_2H_5)_n$ (for n = 1, 2, and 3). In each case, I started the geometrical optimization with the basic arrangement shown in Figure 1, with M---B separations that were close to the sum of the van der Waals radii of boron and the relevant M atom (for M = C, Si, and Ge). [44,45,46]

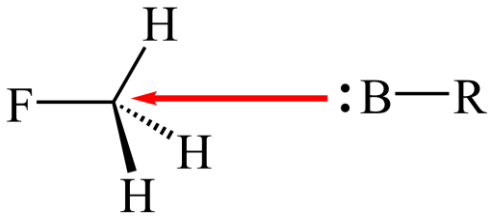

Figure 1. Representation of the starting arrangement used for the optimization of $FH_3M{\leftarrow}{:}BR$ complexes considered in this work. The arrow points to the σ-hole induced by F on the M center and where a dative M−F bond would be formed as BR gets closer.

Singlet or Triple State? Unlike carbenes, where the triplet state is preferred,[47] borylene complexes have been confirmed to prefer the singlet state, as shown in the table below.[22,30,48] The formula: $\Delta E_{(S\text{-}T)} = E_{singlet} - E_{triplet}$, is used for R = H, F, Cl, Br, I, CN, CH_3, and $C(CH_3)_3$. As is seen in Table 1 below, the borylene complexes have a clear

(44) The van der Waals (vdW) radii of B, C, Si, and Ge are 1.92, 1.70, 2.10, and 2.11 Å, respectively, in ref 46.Different sources may list slightly different values for these radii, however. In ref 45, the vdW radii are 2.05, 1.85, 2.25, and 2.23 Å for B, C, Si, and Ge, respectively, with the vdW radius a bit larger for Si than it is for Ge. Even in the latter source, however, the covalent radius of Si is smaller than that for Ge (1.176 and 1.225 Å, respectively).
(45) Batsanov, S. S. *Inorg. Mater.* **2001**, *37*, 871−885.
(46) Atomic Radii of the Elements. In CRC Handbook of Chemistry and Physics, 97th ed.; Haynes, W. M., Ed.; CRC Press: Boca Raton, FL, 2017 (Internet version).
(47) Bauschlicher, C. W., Jr.; Schaefer, H. F., III; Bagus, P. S. *J. Am. Chem. Soc.* **1977**, *99*, 7106−7110.
(48) Brazier, C. R. *J. Mol. Spectrosc.* **1996**, *177*, 90−105.

preference for the singlet state - regardless of the electron donating or withdrawing ability of R in contrast to their carbene analogues (:CH_2 is a triplet but :CF_2 is a singlet). While surprising, our findings are not novel: Bettinger et al. also previously established a preference for the singlet state for other borylene complexes.[22] Therefore for the borylene complexes considered in this work, we only consider the singlet state.

Table 1. Differences in the MP2(full) and CCSD(T) Optimized Singlet and Triplet Zero Point Energy (*ZPE*) Corrected Energies, $\Delta E_{(S-T)} = E_{singlet} - E_{triplet}$, for select Borylene Species[a]

	$\Delta E_{(S-T)}$/eV			$\Delta E_{(S-T)}$/eV	
species	MP2(full)	CCSD(T)	species	MP2(full)	CCSD(T)
:BF	−3.36	−3.62	:BH[b]	−1.00	−1.33
:BCl	−2.27	−2.54	:BCN	−1.31	−1.29
:BBr	−2.06	−2.32	$:BCH_3$	−1.50	−1.76
:BI	−1.79	−2.04	$:BC(CH_3)_3$	−1.48	−[c]

[a]$\Delta E_{(S-T)}$ is negative if the singlet state is preferred. [b]An experimental value of 1.291 eV has been obtained.[48] [c]For $BC(CH_3)_3$, the triplet calculation at the CCSD(T) level failed repeatedly to converge.

σ-hole type interactions. As mentioned previously, the chemistry of borylene complexes has been growing in the past decade, with a focus on their potential as ligands.[16,22,23,49] The forty-two (42) complexes considered in this work were all optimized to (and confirmed to be) minima at the MP2(full) level of theory. Figure 1 shows an arrow pointing to the center of the σ-hole induced on M due to F, i.e. the σ-hole will always be opposite the F-M bond. Fluorine was chosen because fluorine-induced σ-holes are known to be stronger (more positive) than those induced by H, Cl, Br or I.[24,26] Fluorine also has the added advantage of being smaller and less computationally demanding. Figure 2 illustrates the electrostatic potential surfaces of :BF and :BH with arrows pointing to the

(49) Shang, R.; Braunschweig, H. *Inorg. Chem.* **2015**, *54*, 3099−3106.

the F-induced σ-holes (blue region, ***bottom***) and lone pair areas (red region, ***top***) on the boron.

The optimized M---B distances in the FH_3M-BR acid-base pairs are summarized in Table 2. Starting from the general arrangement shown in Figure 1, two distinct bonding motifs emerged:

i. For M = C, the C---B contacts all exceed 3.440 Å, which is slightly shorter than the sum of the van der Waals radii of C and B,[44–46] and well beyond typical covalent C−B bond distances.

ii. For M = Si and Ge, the M−B bonds are all shorter than 3.150 Å, in line with reasonable expectations for dative Si−B and Ge−B bonds.

Very weak electrostatic σ-hole type interactions are formed when M = C, but stronger and shorter dative bonds are achieved when M = Si and Ge. Sigma holes are obviously present on Si and Ge, as shown in Figure 2, but the sigma hole interactions only reinforce the bonding between Si or Ge and N or B, which include a substantial degree of acid←base charge transfer.

Si and Ge have low energy anti-bonding orbitals into which the lone pair electrons of bases can be donated. The separations between the lowest unoccupied and highest occupied molecular orbitals decrease somewhat as well from 18.3 eV for M = C, to 16.7 eV and 16.1 eV for M = Si and Ge. As we show in Table 3, some evidence for the non-covalent character of the C←B bonds, compared to the Si←B and Ge←B is provided by Wiberg bond indices for the optimized sigma hole and dative type structures. The indices are very low (to two decimal places, only 0.01e in each case) when M = C, but they jump by an order of

magnitude when M = Si or Ge (Table 3); they are 0.09 when R = F and increase to 0.25 – 0.30 with the more electron donating alkyl substituents.

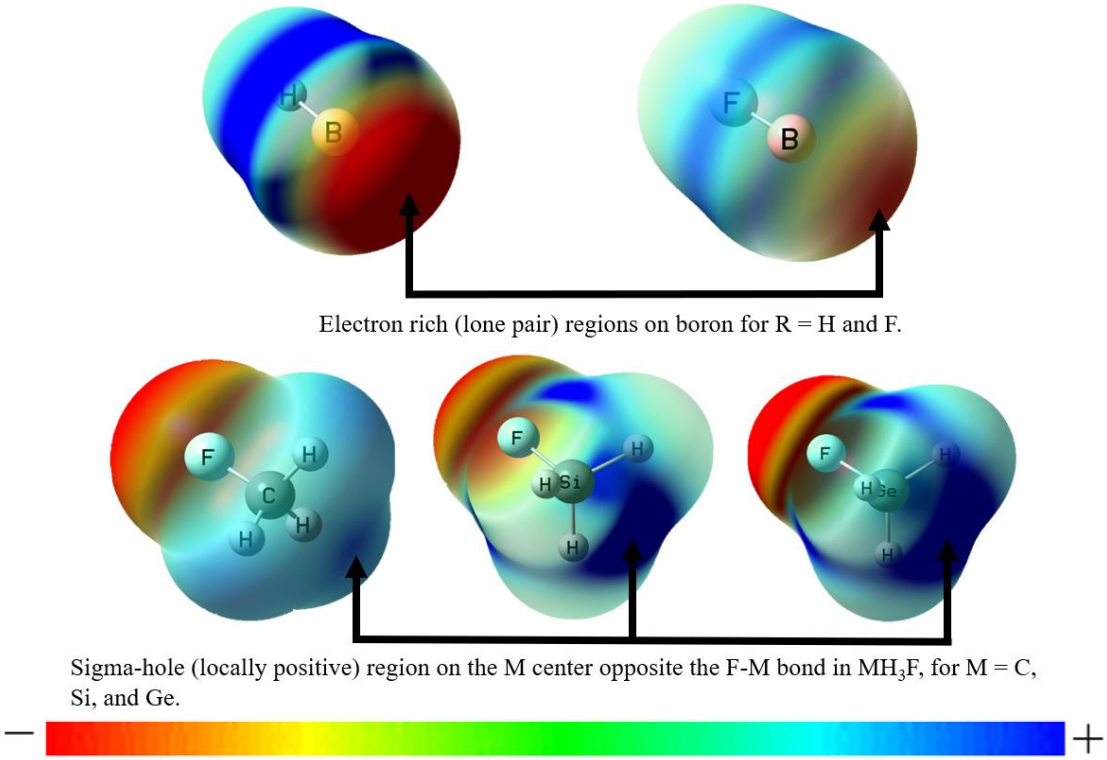

Figure 2. Representations of the electrostatic potentials (ESPs) on the 0.001 au isodensity surface of (top) sample BR bases (for R = H and F). The potential in the region of the lone pair on boron (top) is more negative when R = H vs R = F. The sigma hole on M in $MH_3F$is smallest and weakest for C (bottom). The ESP range is $\pm 3.102 \times 10^{-2}$ au.

Some of the systems that we studied converged to an entirely different bonding motif from the arrangement shown in Figure 1. Those cases are blank in Tables 2 and 3 and will be discussed shortly.

Table 2. M-B distances in weak $FH_3C\leftarrow$:BR and dative $FH_3M\leftarrow$:BR complexes. The data were obtained by optimizing the complexes at the MP2(full) level.

	M---B separation/Å		
substituents	C	Si	Ge
−F	3.480	3.135	3.136
−Cl	3.482	2.995	3.048
−Br	3.441	2.912	3.007
−I	3.478	2.887	3.008
−CN	3.517	2.921	3.032
−H	3.560		2.950
$-C(CH_3)(CH_2)$	3.492		2.756
$-CH_3$	3.525		2.828
$-CH_2CH_3$	3.522		2.794
$-CH(CH_3)_2$	3.519		2.768
$-C(CH_3)_3$	3.512		2.742
$-C(CH_3)_2C_2H_5$	3.511		
$-C(CH_3)(C_2H_5)_2$	3.508		
$-C(C_2H_5)_3$	3.508		

Table 3. Wiberg bond indices for M---B contacts in $FH_3M\leftarrow$:BR complexes obtained from a natural bond orbital (NBO) analysis on geometries optimized at the MP2(full) level.

	M---B bond indices		
substituents	C	Si	Ge
−F	0.010	0.09	0.09
−Cl	0.008	0.12	0.11
−Br	0.009	0.15	0.12
−I	0.008	0.16	0.12
−CN	0.008	0.15	0.12
−H	0.010		0.17
$-C(CH_3)(CH_2)$	0.011		0.27
$-CH_3$	0.010		0.23
$-CH_2CH_3$	0.010		0.25
$-CH(CH_3)_2$	0.010		0.27
$-C(CH_3)_3$	0.011		0.30
$-C(CH_3)_2C_2H_5$	0.011		
$-C(CH_3)(C_2H_5)_2$	0.011		
$-C(C_2H_5)_3$	0.011		

Binding Energies. The basis set superposition error (BSSE) corrected binding energies, ΔE_{bind}, of the acid-base pairs, as shown in Figure 3 below, were calculated using the following equation:

$$\Delta E_{bind} = E(FH_3M \leftarrow\!: BR) - [E(MH_3F) + E(BR)] \qquad (1)$$

These binding energies confirm that the Si and Ge complexes are much more strongly bound than the longer and far less covalent C systems. In fact, the magnitudes of the binding energies for the Si or Ge systems are between 2 and 3 times larger than their M = C analogues.

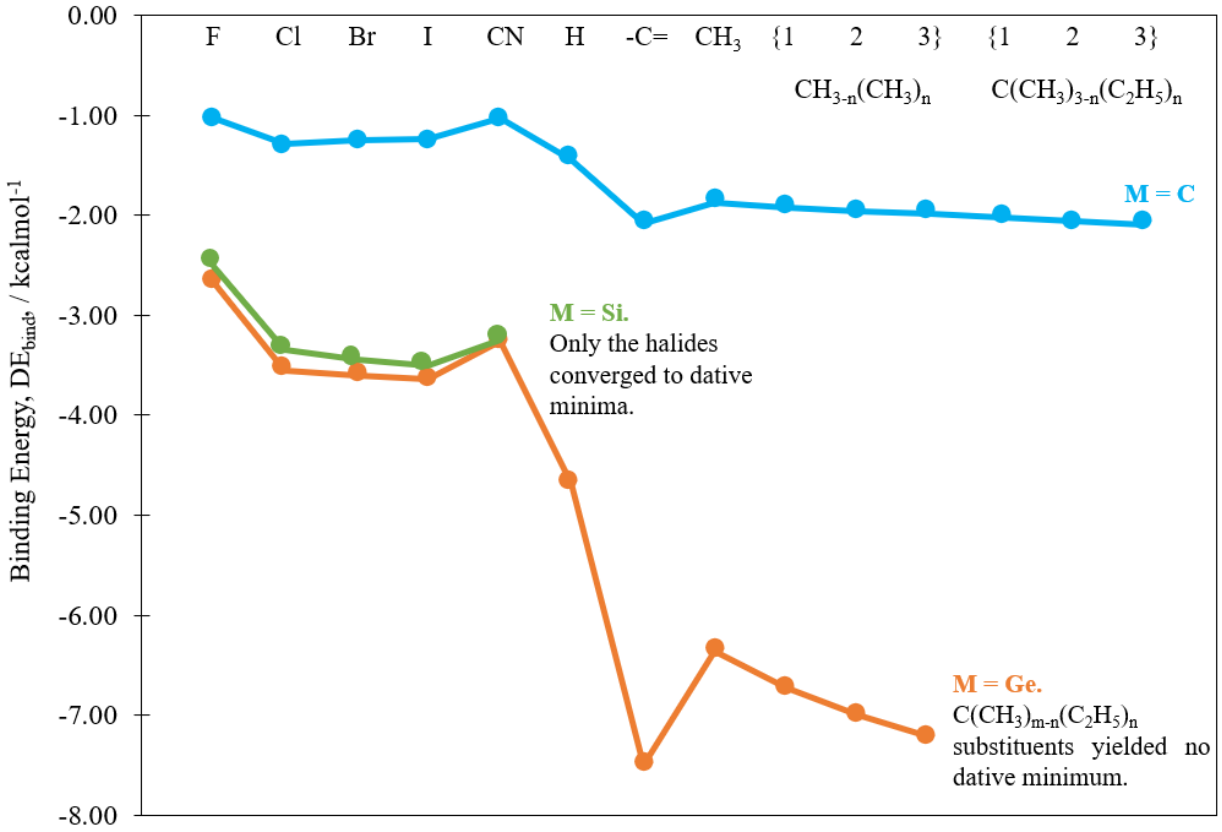

Figure 3. BSSE corrected binding energies, ΔE_{bind}, in kcalmol^{-1}, for the optimized $FH_3M\leftarrow\!:BR$ complexes relative to the isolated acid and base units. "–C=" abbreviates the $CH_2{=}\dot{C}{-}CH_3$ substituent.

The difference in the bonding of the C species vs the Si and Ge complexes are further exemplified in the distance and binding energy data shown in Table 2 and Figure 3: the ***shortest*** and weakest C---B contacts are obtained when R is a halogen atom (or CN). For the other M centers, the ***longest*** and weakest Si−B and Ge−B bond distances are obtained when R is a halogen atom (or CN). The structural data in the latter species are in line with expectations of covalent bonds – weaker bonds tend to be longer (there are, of course, exceptions to this). The longer contacts are explained by the electron withdrawing ability of the R group. These R groups serve to weaken the Si←B and Ge←B donation, leading to the weaker and dative bonds observed. Alternatively, the long C←B interactions can be explained by the contraction of the boron lone pair due to the electron withdrawing power of the halides. This contraction, in turn, allows the halo-borylenes to get closer to the carbon center, still with no significant C←B charge transfer. The exceptional sensitivity of these weak C←B contacts to changes in the immediate chemical environment is evident, in fluctuations in the C←B separations as the halides get larger in Table 2.

Orbital Contributions. We cannot forget to consider the extent of the π-donation from the filled halide p-orbitals to the formally empty 2p orbitals on B. The π-donation serves to stabilize the singlet state for the borylene[22] and competes with M→B back-donation in "M·BR" fragments if M possesses filled valence p- or d-orbitals. In Table 4, we show the Wiberg bond indices for bonds between B and the specific atom in R to which it is bonded. The net charge on B and the extent of the involvement of the σ hybrid and unoccupied π orbitals of B in the BR bond are included. The data were obtained from NBO analyses; the orbital involvement is quantified as a percentage derived from the square of

the polarization coefficient, c_B, for a given σ or π orbital: $c_B^2 + c_A^2 = 1$. The NBO analysis uncovered π contribution to the bonding with B only for the halo-borylenes. The cases for R = CN or $CH_3{-}C{=}CH_2$ in which the B is bonded to an unsaturated C center showed no significant π involvement.

Table 4. MP2(full) NBO charges on B in free BR, Wiberg bond indices for bond directly linking B to R, and square of the boron hybrid σ and π coefficients in percentages (for σ donation from B and π donation to B). For polyatomic R groups, the specific atom to which B is bonded is in italics.

R	q/e	WBI	σ(s−p)/%	$\pi(p_x)$/%	$\pi(p_y)$/%
F	0.54	0.76	11	5	5
Cl	0.26	1.13	22	7	7
Br	0.20	1.21	24	8	8
I	0.11	1.29	26	8	8
*C*N	0.46	0.75	23		
H	0.36	0.84	32		
$CH_3{-}C{=}CH_2$	0.42	0.75	23		
CH_3	0.48	0.75	23		
CH_2CH_3	0.49	0.72	23		
$CH(CH_3)_2$	0.52	0.68	22		
$C(CH_3)_3$	0.56	0.62	20		
$C(CH_3)_2C_2H_5$	0.56	0.60	20		
$C(CH_3)(C_2H_5)_2$	0.57	0.59	19		
$C(C_2H_5)_3$	0.59	0.57	18		

Insertion vs. Coordination. As briefly mentioned earlier, many of the complexes considered in this work converged to an entirely different bonding motif than expected. These complexes include the BR bases with organic R substituents for M = Si and BR bases with the largest R substituents, $(C(CH_3)_{3-n}(C_2H_5)_n)$, for M = Ge. For those acid-base pairs, the initial arrangement shown in Figure 1 converged to an insertion product FH_2M-BHR with a trivalent boron center – which involved a M-H bond activation. The different bonding motifs observed in this work are shown below in Figure 4.

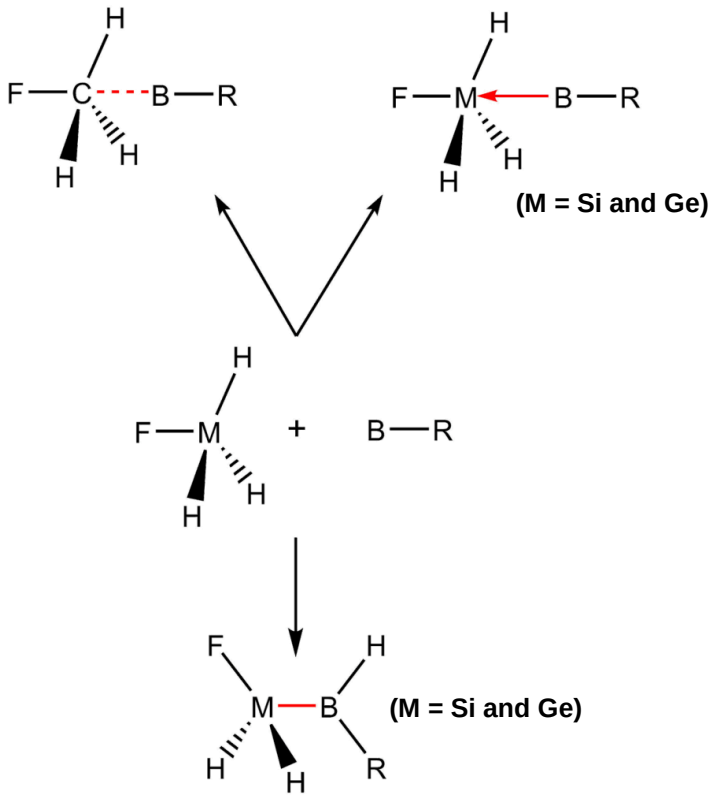

Figure 4. Products obtained by optimizing FH_3M + BR acid-base pairs, starting with M---B separations ≈ sum of the van der Waals radii. Outcomes: (***top left***) weak van-der Waals type complex for M = C, (***top right***) dative covalent complex formed for M = Si and Ge with the more electron withdrawing R groups, and (***bottom***) the B-R insertion product formed by all other Si and Ge systems. The outcomes have been confirmed via NBO analyses.

Figure 3 establishes which acid-base pairs converged to a weak van-der Waals type or dative covalent complex as illustrated in Figure 4 (Figure 4, ***top***). The assumption made is that the complexes not shown in Figure 3 collapse directly to the insertion product (Figure 4, ***bottom***). This inference has been confirmed via NBO analysis. Computed M-B distances for FH_2M-BHR compounds are listed below in Table 5. For completeness, we directly optimized FH_2MBHR molecules for M = C, Si, and Ge, for all fourteen R groups. For the cases where the complexes did not collapse directly to the covalent molecule, we

started the optimizations with guess structures in the geometry of Figure 4 (***bottom***) with estimated covalent bond distances.

Table 5. MP2(full) covalent M-B distances in FH_2M-BHR. The data in bold highlights the systems that converged directly to the insertion product.

	M---B Separation / Å		
Substituents	**C**	**Si**	**Ge**
-F	1.566	2.031	2.055
-Cl	1.558	2.011	2.037
-Br	1.556	2.006	2.033
-I	1.555	2.002	2.029
-CN	1.550	2.010	2.034
-H	1.549	**2.002**	2.028
$-C(CH_3)(CH_2)$	1.559	**2.009**	2.032
$-CH_3$	1.556	**2.007**	2.034
$-CH_2CH_3$	1.557	**2.007**	2.036
$-CH(CH_3)_2$	1.557	**2.004**	2.031
$-C(CH_3)_3$	1.557	**1.880**	2.032
$-C(CH_3)_2C_2H_5$	1.559	**2.002**	**2.035**
$-C(CH_3)(C_2H_5)_2$	1.559	**2.011**	**2.028**
$-C(C_2H_5)_3$	1.560	**2.012**	**2.036**

The Decline and Fall of Barriers. As seen in Table 5, the complexes considered in this work all possess an insertion product. This is in stark contrast to the coordination bonding motif which was seen for all species except for the extremely electron donating groups for M = Si and the largest alkylboranes for M = Ge. One thing to note: the borylenes that formed the strongest C←B and Ge←B interactions, also achieved direct Si-H activation leading to the insertion product. This implies the existence of a binding energy cut-off for the coordination complexed, beyond which M-H activation is stabilized relative to simple coordination such that the latter is not a favored arrangement at all and ceases to

be a minimum on the potential energy surface. Based on Figure 3, this cut-off for M = Si is low (somewhere between 4 – 5 kcal/mol), whereas for M = Ge, the cut-off appears much later.

The tendency towards BR insertion increases as R becomes more electron donating (beyond R = CN in Figure 3) and is a result of the lone pair on B becoming more available. If we think about this in terms of carbene chemistry,[50,51,52] the halo-borylenes are better nucleophiles for interactions to the vacant boron p-orbitals due to π contributions from the halides, but they are worse σ-donors (nucleophiles) for dative interactions or, ultimately, insertion. The reverse is generally true for the alkyl substituents. Even though, as pointed out in ref. 22, hyperconjugation by alkyl substituents can also influence p-orbital occupation on the B center, the alkyl substituents are good σ-donors. Consequently, the alkyl-borylenes coordinate more strongly to M as σ-donors in dative bonds. As the M←B interaction becomes stronger, however, and the M-B contacts in the minimum energy structures shrink, the prospect for CH activation is greatly enhances.

The short M-B contact aids the proton transfer from M to B via the donation of B lone pair into a low energy orbital on MH_3F and the initial donation from the M-H bond into an empty p orbital on B. The resulting insertion product has the double thermodynamic advantage of oxidizing the monovalent boron to the preferred trivalent form and sacrificing one covalent (M-H) bond for two new ones – a M-B and a B-H bond.

(50) Moss, R. A.; Mallon, C. B. *J. Am. Chem. Soc.* **1975**, *97*, 344−347.
(51) Moss, R. A. *Acc. Chem. Res.* **1980**, *13*, 58−64.
(52) Moss, R. A Carbenic Philicity. In Carbene Chemistry: From Fleeting Intermediates to Powerful Reagents; Bertrand, G., Ed.; Fontis Media: Chapter 3, pp 57−101.

Reaction Paths. To understand the tendency towards borylene insertion, we carried out IRC path calculations at the MP2(full) level for all five of the cases (R = F, Cl, Br, I, and CN) for which FH_3M←BR type complexes were obtained for M = C, Si, and Ge. The IRC calculations were preceded by relaxed potential energy surface scans that gave us a general picture of the energy changes leading to insertions and allowed us to obtain reasonable guess structures for transitions states. The guess transition state structures obtained from the scans were employed in QSTn calculations and the transition state structure candidates obtained in that way were re-optimized to confirm that they were first order saddle points. The transition state structures that were found to link the coordinated CFH_3 and BR systems (Figure 4, ***top***) to the insertion product (Figure 4, ***bottom***) are shown in Figures 5 and 6. They are quite similar to structures identified in refs 22 and 23 for borylene insertion into the CH bonds of methane. The IRC path calculations were conducted using those confirmed structures. Figure 7 shows the proposed dehydrohalogenation pathway observed in potential energy scans.

For M = Si and Ge, the transition states found are close geometrically to the latter form for M = C, and examples are shown in Figure 6 for the fluoride, iodide, and cyano bases. The transition structures are unique for M = C for the BR insertion (cf. Figures 5 and 7), and the associated energy barriers are remarkably high compared to the Si and Ge systems (Figure 6). The differences in the transition states suggest a fundamental difference in the mechanism of the reactions for M = C, vs. M = Si and Ge, and that difference is summarized in Figure 8.

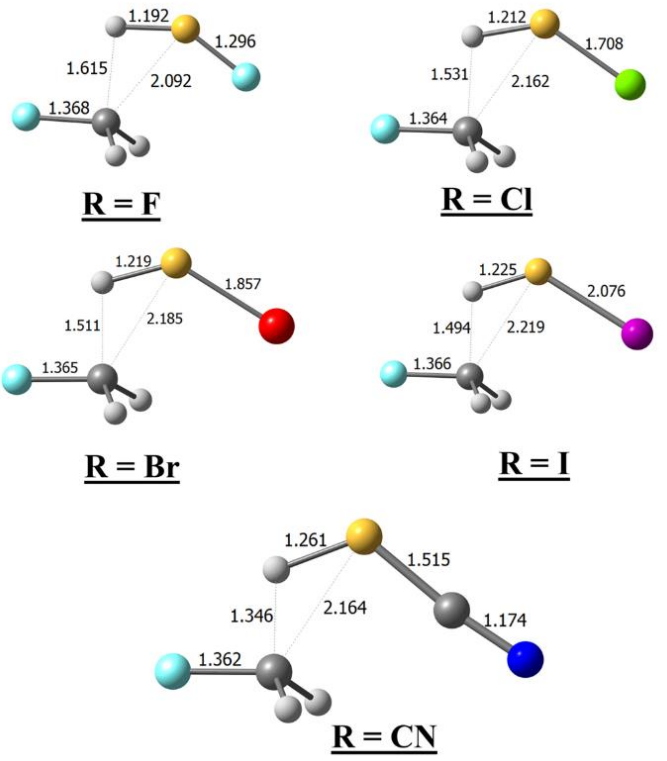

Figure 5. Transition state structures linking the van der Waals and covalent minima on the potential energy surface of MH_3F + BR, for M = C and R = F, Cl, Br, I, and CN.

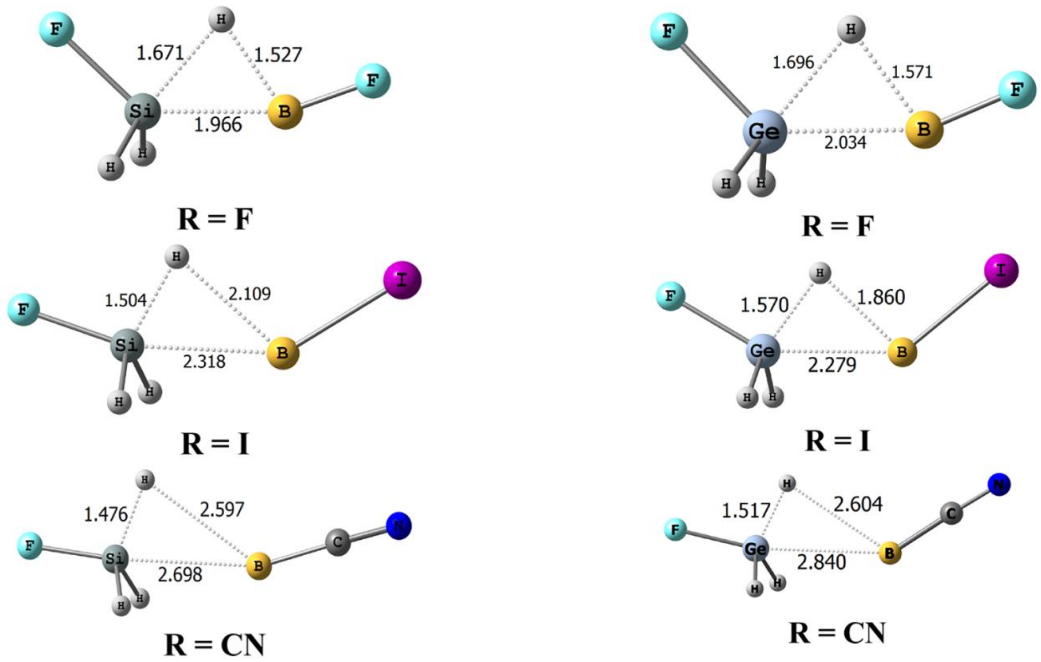

Figure 6. Transition state structures linking the dative and covalent minima on the potential energy surface of MH_3F + BR for M = Si and Ge, and R = F, I, and CN. The cases shown here are qualitatively identical to those for R = Cl and Br.

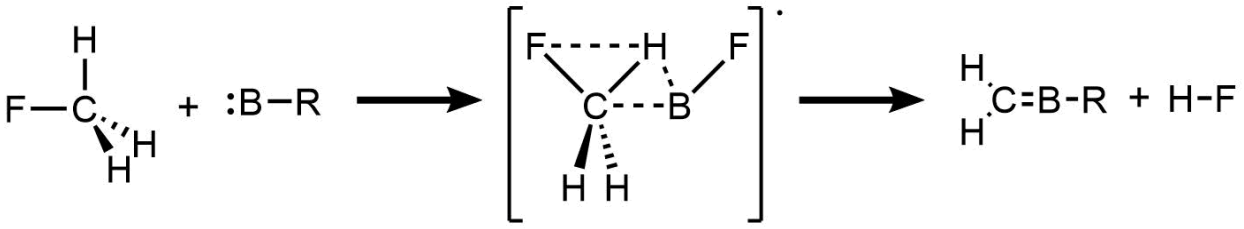

Figure 7. Alternative insertion pathway observed in potential energy scans and IRC calculations for some cases when M = C.

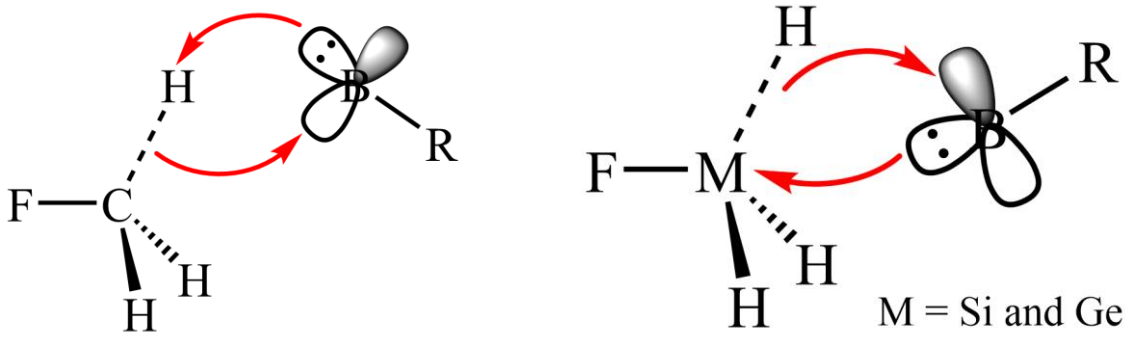

Figure 8. Mechanistic differences between the BR insertion for M = C (***left***), and for M = Si and Ge (***right***). For clarity we exclude one of empty p orbitals on B.

The insertion occurs for C, as shown in Figure 8 (***left***), by a donation of the B lone pair to the terminal H, and a donation of the electrons of the activated C−H bond to an empty B p-orbital. For the polarized and more electropositive Si and Ge centers, however, the B lone pair is donated to the M center, leading to M−H activation and H migration to the B center (Figure 8, ***right***). Figure 9 shows the IRC paths obtained for the halide and cyano substituents that converged to dative type minima for each metal center.

Quantifying the Barriers. The IRC paths do not necessarily terminate, on either side of Figure 9, to fully optimized geometries, so we list in Table 6 the differences in the free energies of the optimized FH_2M−BHR and the optimized weakly bound C or dative Si and Ge structures, ΔG, for the five R groups.

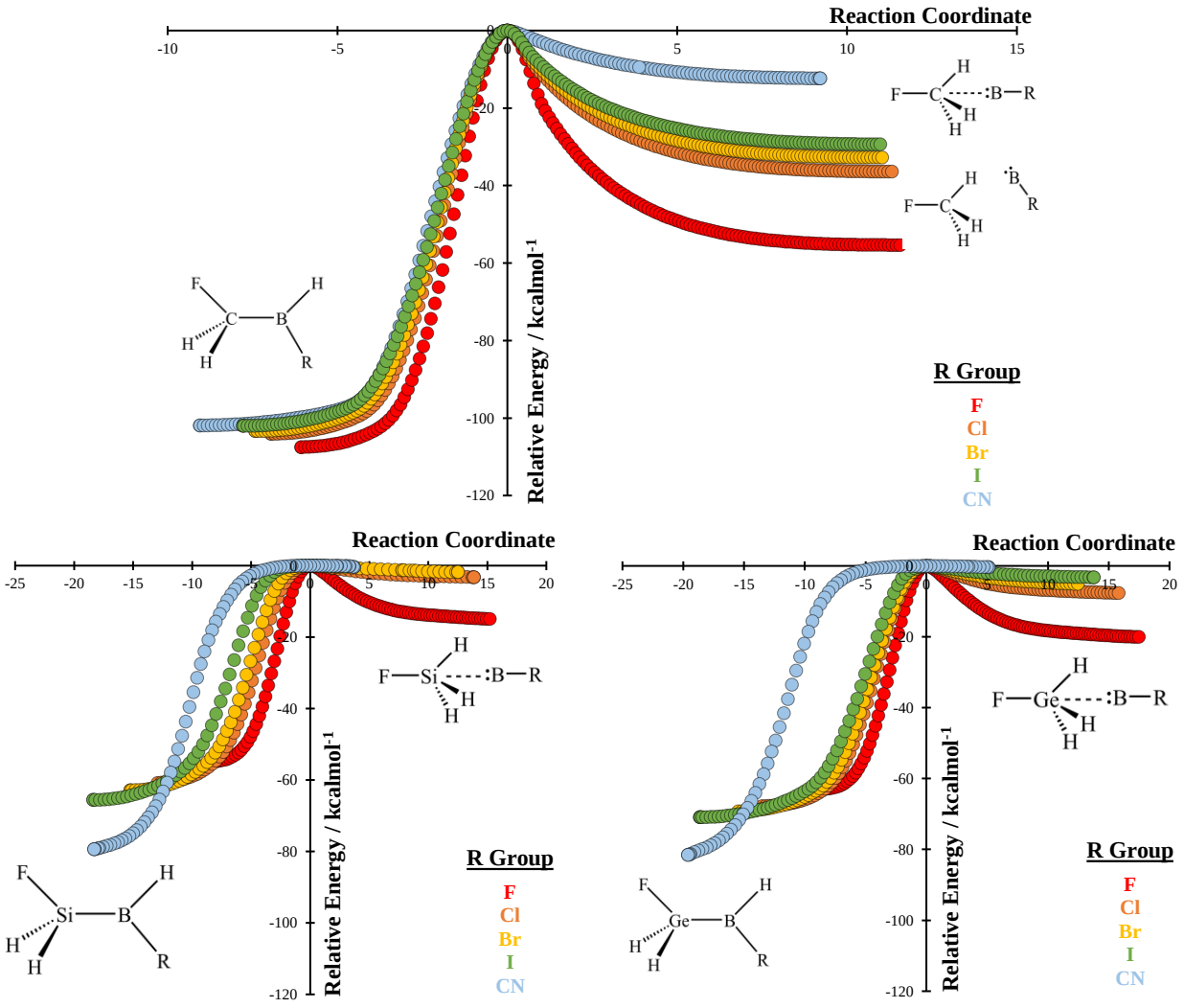

Figure 9. IRC paths obtained at the MP2(full) level of theory linking the insertion product FH_2MBHR (*left*) to the more weakly bound FH_3M---BR pairs (*right*) for M = C, Si, and Ge, and R = F, Cl, Br, I, and CN. For M = C, the IRCs terminated in several cases at weak dipole-dipole or van der Waals type complexes as illustrated in the C graph on the right.

Table 6. MP2(full) Free energy changes going from weak or dative (Dat) type complexes to FH_2MBHR ($\Delta G_{Dat-Cov}$) and from the covalent (Cov) and dative type structures to the transition structure (TS). All values are in kcalmol^{-1} units.

	ΔG(Dat−Cov)			$\Delta G^{\ddagger}$(TS−Cov)			$\Delta G^{\ddagger}$(TS−Dat)		
R	C	Si	Ge	C	Si	Ge	C	Si	Ge
F	46.9	37.1	40.0	104.0	53.5	61.7	57.1	16.4	21.7
Cl	62.3	54.3	56.8	101.0	59.4	66.3	38.6	5.1	9.5
Br	65.6	58.1	60.5	100.3	61.3	67.7	34.7	3.2	7.2
I	67.8	61.9	64.1	99.0	63.7	69.1	31.2	1.8	5.0
CN	83.9	76.0	78.5	99.4	76.9	79.9	15.4	0.9	1.4

Table 6 shows that the energy barrier going from the dative structures (Figure 8, right) is highest for M = C, and lowest for Si, with the Ge barriers in the middle, even if they are only slightly higher than those for Si. For R = CN, the journey to the covalent structure (right to left in Figure 8) is nearly barrierless for both Si and Ge but quite high for C. The largest barrier for each M is obtained when R = F. As R gets heavier and less electronegative, the borylene becomes more nucleophilic, making the lone pair more available for σ-donation. As a result, the barriers fall – slowly for C, and rapidly for Ge and Si.

Table 6 also highlights the thermodynamic and kinetic favorability of the Dat→Cov reaction as the R substituent becomes more and more electron donating, such that in the case of BCN, the reaction appears to be barrierless for Si and Ge – 0.9 $kcalmol^{-1}$ and 1.4 $kcalmol^{-1}$ respectively. This shows that the Dat→Cov reaction becomes barrierless when the R substituent becomes even more electron donating, which accounts in fact for our failure to find dative minima in most cases for Si and some cases for Ge (cfs. Figure 3 and Tables 2 and 3).

Barrierless Convergence. To study the formation of FH_2SiBHR for all fourteen bases, we carried out IRC calculations following the protocol mentioned above, using, in this case, the B3LYP-D3 method. The outcomes are summarized in Figure 10. The data are very close qualitatively to those obtained at the MP2(full) level. For the C, Si and Ge systems with dative minima, we started the IRC path calculations from the B3LYP-D3 optimized transition state structures. For the Si and Ge that had no dative minima we carried out 'downhill' IRC path calculations starting from long M---B separations equal to ~3.5 Å.

In a few cases where the potential energy surface was very flat, we accepted slightly shorter separations, still well beyond the sum of the M and B van der Waals radii for the IRC calculations.

The most impressive observation from the IRCs for the latter systems is the barrierlessness of the insertion. That observation helps us to understand why no dative species was located in those cases. If the substituent is sufficiently electron donating and M is sufficiently electrophilic, the barrier to insertion shrinks and, for M = Si, and easily disappears.

The computed energy and free energy differences for the optimized weak and dative type pairs and insertion products relative to the transition state structures for the cases in Figure 8 are shown in Table 6 below. Unlike the Si cases for R = H and CH_3, barriers are actually observed (though low) when M = Ge. The same basic pattern (low barriers for Ge and none for Si) is observed in Table 7 for the other R groups as well where persistent dative minima when observed for Ge, but not for Si. We compare in Figure 10 the IRC graphs shown in Figure 11 for two sample cases (R = CH_3, where there is no barrier for Si and a very small barrier for Ge, and R = F with the largest barriers in each case). This allows for a direct comparison and a graphical representation of the effects of changing M on the nature of the potential energy surfaces.

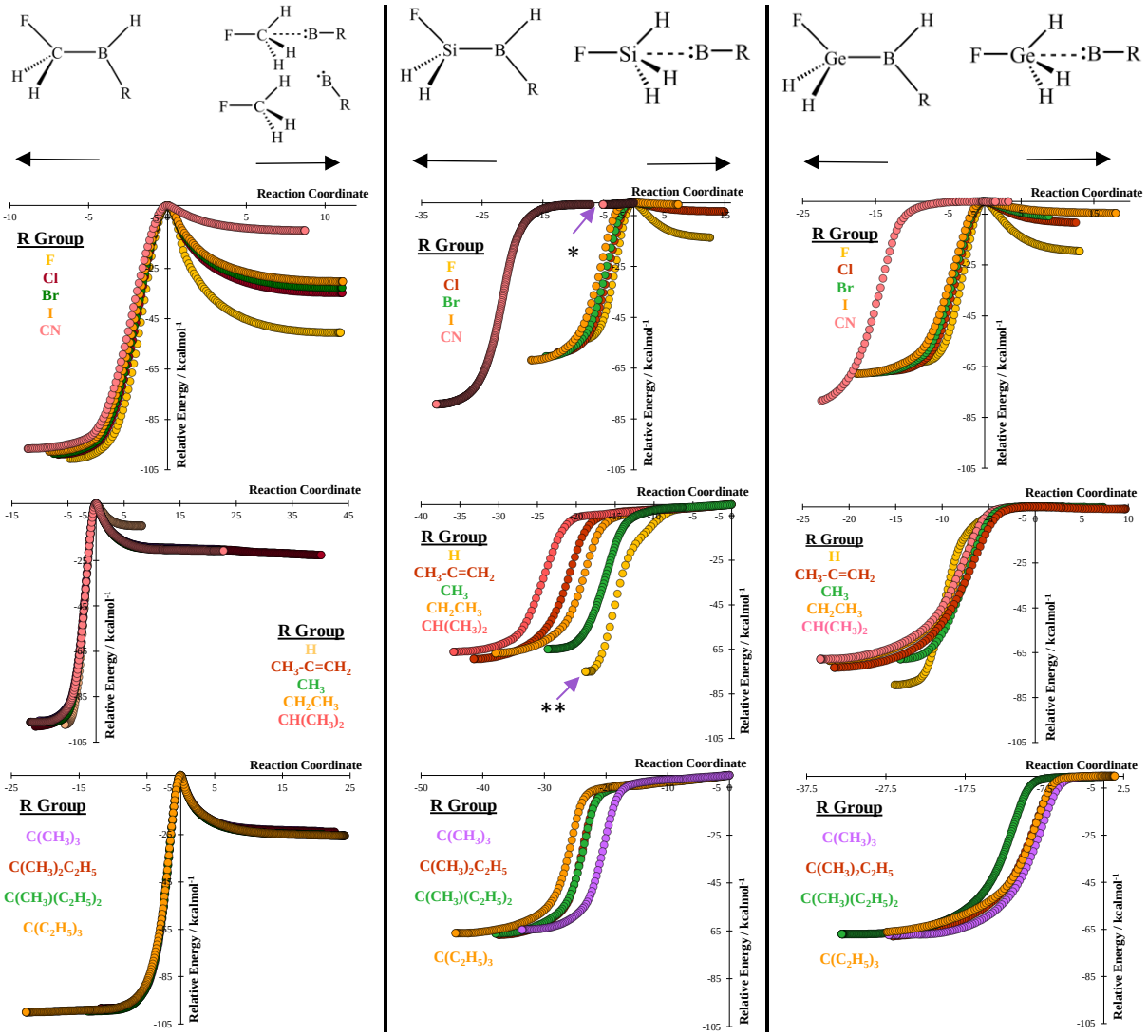

Figure 10. B3LYP-D3 IRC paths for the interactions of BR bases and MH_3F for M = C, Si, and Ge. *For SiH_3F + BCN (***top, center***) the IRC path terminated initially at a dative second-order saddle point. We continued the optimization with a new input obtained by following one of two degenerate bending vibrations with imaginary frequencies. **For SiH_3F + BH (***middle***, ***center***), the usual product ($FH_2Si{-}BH_2$) transformed in the last few IRC steps to a product with one of the H atoms bonded to Si moved into a bridging position above the Si−B bond.

As the base gets more electron donating and the boron lone pair becomes more available, the potential energy surface for M = Ge becomes flat. But why is the base insertion so effortless for Si?

Table 7. B3LYP-D3 Free Energy Differences (ΔG) for the Covalent (Cov), Dative (Dat) and Transition State Structures (TS)[a]

	ΔG(Dat−Cov)			$\Delta G^{\ddagger}$(TS−Cov)			$\Delta G^{\ddagger}$(TS−Dat)		
R	C	Si	Ge	C	Si	Ge	C	Si	Ge
F	44.8	36.0	38.7	97.1	52.4	61.6	52.4	16.4	22.9
Cl	58.7	51.6	53.7	95.9	57.5	65.1	37.1	5.9	11.4
Br	60.7	54.3	56.2	95.7	58.9	65.7	35.0	4.6	9.5
I	62.4	57.0	58.7	94.8	60.2	65.9	32.5	3.2	7.2
CN	80.5		75.4	93.7		77.0	13.2		1.6
H	81.1		74.6	94.4		75.5	13.3		0.9
CH_3−C═CH_2	70.4		65.2	94.6		69.0	24.1		3.8
CH_3	67.2		61.7	93.4		65.4	26.2		3.6
CH_2CH_3	67.7		63.0	92.7		66.3	25.0		3.4
$CH(CH_3)_2$	67.8		61.7	93.5		65.1	25.8		3.4
$C(CH_3)_3$	67.5		61.6	95.5		64.6	28.0		3.0
$C(CH_3)_2C_2H_5$	66.5		62.0[b]	95.1		64.0[b]	28.5		2.0[b]
$C(CH_3)(C_2H_5)_2$	66.6			95.8			29.1		
$C(C_2H_5)_3$	67.0		61.8[b]	96.5		63.2[b]	29.4		1.5[b]

[a]All values are in kcalmol^{-1}. [b]The complexes formed by these two systems with shorter dative bonds for M = Ge had F−M−B bond angles that were tilted noticeably from the 180° alignment that is typical for σ-hole supported interactions. They were 171.6° and 166.7° for $C(CH_3)_2C_2H_5$ and $C(C_2H_5)_3$, respectively. We located no minimum for $C(CH_3)(C_2H_5)_2$.

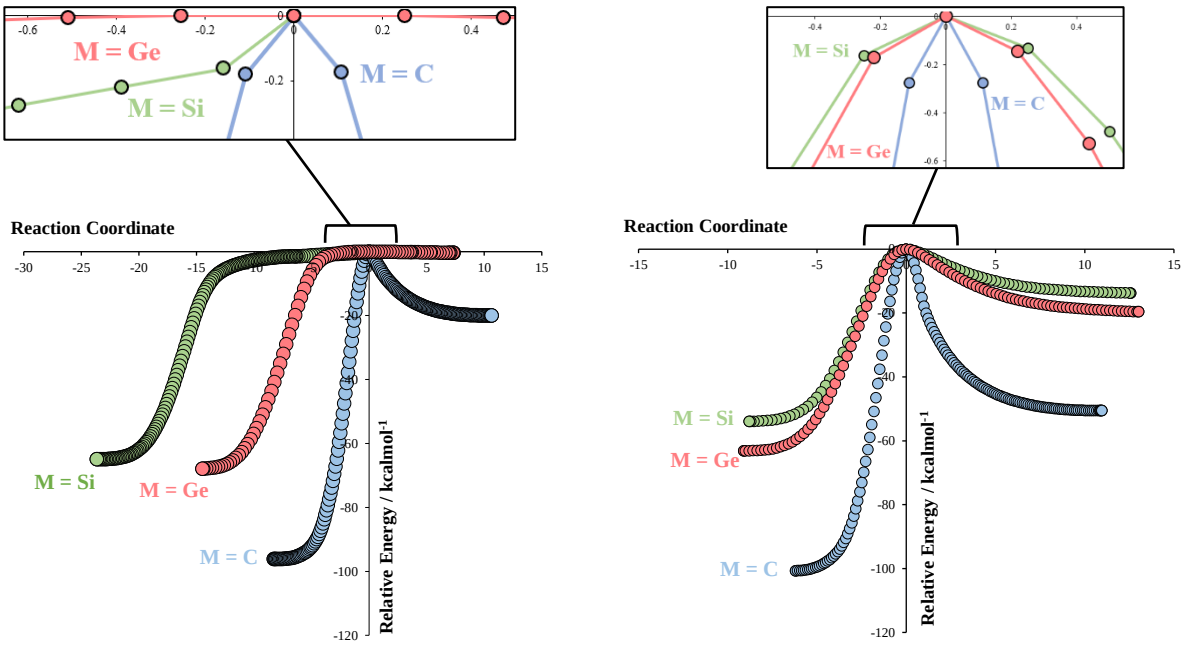

Figure 11. IRC paths for the reaction of two borylene bases (BR, for R = CH_3 [***left***] and F [***right***]) with MFH_3 (for M = C, Si, and Ge) to form FH_2M-BHR.

The exceptional behavior for silicon reflects the generally anomalous character of Si in group 14, it's more electropositive (and electrophilic) character compared to C and

arguably Ge, the smaller HOMO-LUMO gap mentioned above and the larger atomic size compared to C. On the Pauling scale, the electronegativity, χ, of Si is lower than those of both C and Ge, with χ^{P}_{Si} slightly smaller than χ^{P}_{Ge}. That order is reversed on the basic Mulliken electronegativity ($\chi^{M}_{Si} > \chi^{M}_{Ge}$ for the isolated atoms), but the more relevant tetrahedral valence state Mulliken electronegativities[53] are in full agreement with the Pauling scale that $\chi_{C} > \chi_{Ge} > \chi_{Si}$. On the corresponding valence state chemical hardness scale,[53] the Si atom is also the softest of the three atoms. And, given that softness varies directly with polarizability,[54] it is not surprising that the size and strength of the sigma hole on M increase substantially going from C to Si, and are comparable for Si and Ge.

The relative availability of low energy orbitals on Si and Ge makes it possible for stable dative interactions (supported by the presence of a strong sigma hole in MH_3F) with BR. But, as the lone pair on B becomes more available, the interaction between the boron center and the M center (and the relevant vicinal hydrogens on the M center if the M-H bond is short enough) becomes stronger. Si is slightly smaller than Ge (especially as a formally 4+ cation)[45,46,55] and is ostensibly more electropositive than Ge due to the influence of d-orbital contraction on Ge such that the M-H interaction (i) is more stabilizing and (ii) happens earlier on as R becomes more electron donating. As a result, BR insertion is simple when M = Si, except in cases where BR is a poor base due to the electron-withdrawing power of R and a compromised Lewis acid due to B←R π-donation.

(53) Bratsch, S. G. Revised Mulliken Electronegativities - I. Calculation and Conversion to Pauling Units. J. Chem. Educ. 1988, 65,34−41. The valence state Mulliken electronegativities for tetravalent C, Si, and Ge are 8.15, 7.30, and 7.53 eV, respectively.
(54) Fuentealba, P.; Reyes, O. *J. Mol. Struct.: THEOCHEM* **1993**, *282*, 65−70.
(55) Pyykkö, P. *J. Phys. Chem. A* **2015**, *119*, 2326−2337.

Ge is similar in many of these respects to Si, but the collapse in the barrier to insertion is postponed for Ge to the most nucleophilic cases, even if the barriers in many cases are miniscule (Table 7). Overall, the structural and electronic evidence suggests that the lower barriers to BR insertion into the Si-H bond relative to C-H and Ge-H bonds are achieved by a conspiracy of subtle physico-chemical properties and not by any single aspect of the bonding in SiH_3F.

Conclusion

The nature of dative and sigma hole type interactions by monovalent boron (B-R) as a base has been investigated. I find that the electron deficiency of boron in B-R opens up an alternative (better yet, competing) channel for bonding. I find that for Lewis acids with the general formula FH_3M, where M = C, Si, and Ge, BR insertion into one of the M-H bonds to form FH_2M-BHR is barrierless in most case for M = Si, and for Ge, too, when BR is sufficiently nucleophilic. For M = C, the barriers are relatively high.

We can say that this barrierless insertion is promoted by (i) increasing the electrophilic character of the M center, and (ii) increasing the nucleophilic character on the base, which depend on the electron donating ability of the R group. For the halo-borylenes, BR is weakened as both a Lewis acid (due to π contributions from R to the valence p-orbitals of B; Table 4) and as a Lewis base (due polarization) by the halides.

Nonetheless, as soon as the conditions become more favorable – where the sigma hole on M is strong, low energy empty orbitals are available on M for charge transfer, and the base is a nucleophilic enough, BR insertion is barrierless and dative bonding is sidestepped such that the dative system is not even as a local minimum. Different

mechanisms are implied by the transition state structures that we observe, see Figures 7 and 8.

For the various Ge systems where the barriers are present but very low, the likelihood of GeH activation and BR insertion is expected to very sensitive to the actual thermodynamic conditions. The experimental evidence that is available to date, however, shows that barriers to insertion for organic and organometallic compounds are surmountable under reasonable reaction conditions. The barriers, where they exist at all, should be even more readily transgressed for Si and Ge. C-H bond activation is hardest to achieve, but examples of bond activation for other organic species is encouraging for the future of borylene mediated chemistry in organic synthesis under appropriate conditions.

Chapter 3

Ongoing Projects

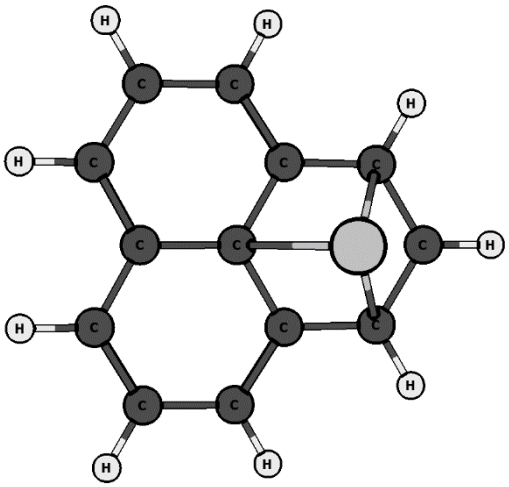

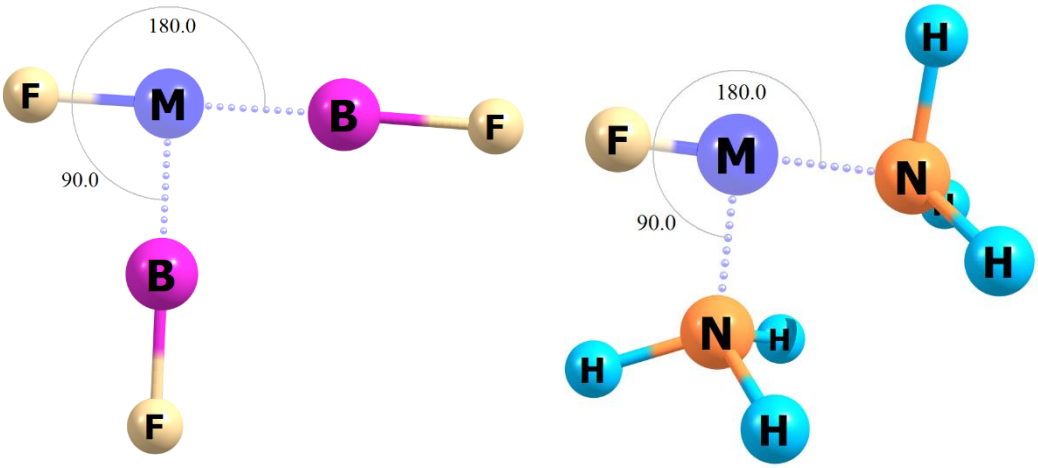

Abstract

In this chapter, I discuss two ongoing projects, the goals of each, as well as preliminary results and future work to be done.

1. Fluxional Behavior in Half-Sandwich Complexes of the Phenalenyl Radical

The phenalenyl radical (***P*** = $C_{13}H_9$·) is a relatively stable, organic radical comprised of three fused, six membered rings sharing a central carbon. This system is especially interesting because it combines the properties of the six-membered benzene ring and the radical character of Cp. In this work, I analyze the thermodynamic and kinetic stability of two sets of phenalenyl complexes: (i) ***P***M (M = Li, Na, K, Rb, Cs, Sc, Ti, V, and Cr) and (ii) ***P***MX_n where M = Sc, Ti, V, Cr, X = F, Cl (n = 2 when M = Sc and V, and n = 3 when M = Ti and Cr). The high symmetry of the phenalenyl ring (D_{3h}) suggests that in cases where the barriers to translation across the surface of the molecule are low, fluxional behavior may be observed. I report the outcome of a series of investigations into the fluxionality of these complexes.

2. Investigations into σ-hole Interactions and Consequences for Structure

A σ-hole is an electron-deficient outer lobe of a half-filled p (or nearly p) orbital involved in forming a covalent bond. If this electron deficiency is sufficient, a region of positive (or relatively positive) electrostatic potential will result which can then noncovalently interact with negative sites on other molecules. These interactions are highly directional, as their ability to adopt certain geometric patterns with a higher likeliness than others is one of their most characteristic properties. That is to say, σ-holes represent a structure-determining force, and the nearly linear arrangement is a consequence. But the question certainly arises: to what extent does a linear arrangement strengthen the σ-hole interaction? In this work, I report the effect of directionality on the σ-hole interaction between M-F (M = Li, Na, K, Cu, Ag, and Au) compounds and well-known electron donors (D = BF and NH_3).

Fluxional Behavior in Half-Sandwich Complexes of the Phenalenyl Radical

Introduction

The phenalenyl (***P***) radical = $\cdot C_{13}H_9$ (Figure 1), is a planar structure comprised of three fused six membered rings sharing a central carbon. The electronic structure of the tricyclic system itself has been well studied computationally,[1,2,3] but its organometallic chemistry is underdeveloped despite its as a radical,[4] cation,[5] and anion.[6] That characteristic has made related compounds extremely useful for exploring new conjugated electronic structures,[7,8,9,10,11,12,13,14,15] but the phenalenyl radical itself has not been characterized in the solid state because of its easy dimerization and air oxidation.[7] In a localized representation, the structure of ***P*** may be drawn with the radical electron located at the central carbon (9a in Figure 1). Other resonance structures place the unpaired electron along the outer carbons or at symmetrically identical positions around the ring, however, calculations at various levels of theory show that the singly occupied molecular orbital (SOMO) has in fact an electron density of zero at the central atom,[3,17] and is a nonbonding A_1" molecular orbital.[16]

(1) Haddon, R.C. *Journal of Chemistry* **1975**, *28*, 2343-2351.
(2) Goto, K.; Kubo, T.; Yamamoto, K. et al. *J. Am. Chem. Soc.* **1999**, *121*(7), 1619-1620.
(3) Fukui, K.; Sato, K.; Shiomi, D. et al. *Synthetic Metals* **1999**, *103*(1-3), 2257-2258.
(4) Boekelheide, V.; Larrabee, C. E. *J. Am. Chem. Soc*. **1950**, *72*, 1245-1249.
(5) Pettit, R. *J. Am. Chem. Soc.* **1960**, *82*, 1972-1975.
(6) Kubo, T.; Yamamoto, K. et al. *Angew. Chem., Int. Ed*. **1996**, *35*, 439-441.
(7) Nakasuji, K.; Yoshida, K.; Murata, I. *J. Am. Chem. Soc.* **1982**, *104*, 1432-1433.
(8) Nakasuji, K.; Yoshida, K.; Murata, I. *Chem. Lett.* **1982**, *11*(7), 969-970.
(9) Nakasuji, K.; Yoshida, K.; Murata, I. *J. Am. Chem. Soc.* **1983**, *105*, 5136-5137.
(10) Murata, I.; Sasaki, S.; Klabunde, K.-U.; Toyoda, J.; Nakasuji, K. *Angew. Chem., Int. Ed.* **1991**, *30*, 172-173.
(11) Ohashi, K.; Kubo, T.; Masui, T.; Yamamoto, K.; Nakasuji, K.; Takui, T.; Kai, Y.; Murata, I. *J. Am. Chem. Soc.* **1998**, *120*, 2018-2027.
(12) Haddon, R. C. *Nature* **1975**, *256*, 394-396.
(13) Haddon, R. C.; Wudl, F.; Kaplan, M. L.; Marshall, J. H.; Cais, R. E.; Bramwell, F. B. *J. Am. Chem. Soc*. **1978**, *100*, 7629-7633.
(14) Haddon, R. C.; Chichester, S. V.; Stein, S.M.; Marshall, J. H.; Mujsce, A. M. *J. Org. Chem.* **1987**, *52*, 711-712.
(15) Hatanaka, K.; Morita, Y.; Ohba, T.; Yamaguchi, K.; Takui, T.; Kinoshita, M.; Nakasuji, K. *Tetrahedron Lett.* **1996**, *37*, 873-880.
(16) Reid, D. H. Quart. Rev. (London) 274, 19, 1965. Section 4.4, pp 286-288.

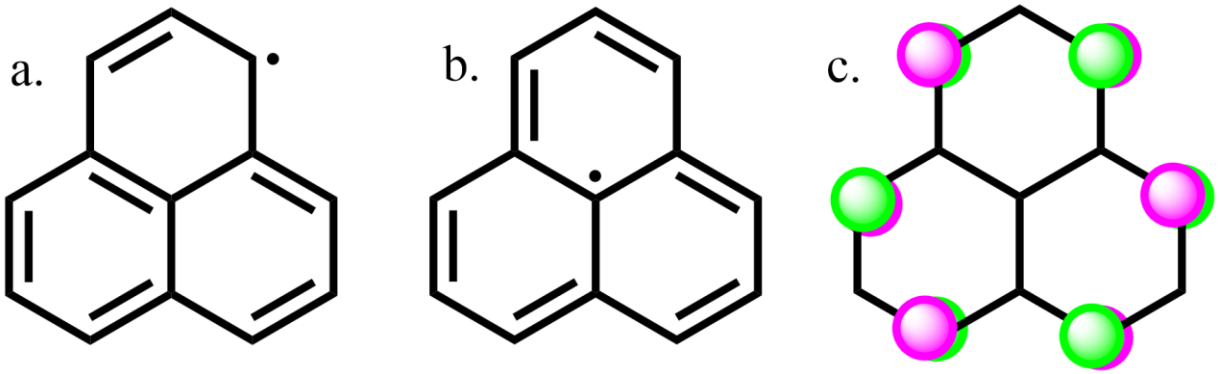

Figure 1. Localized representations (two resonance structures and the SOMO) of the phenalenyl radical, ***P***.

The nature of the frontier singly occupied molecular orbital (SOMO) of the radical has been shown to be key to understanding the observed plurality in the coordination preferences in M***P***$_2$.[9] The SOMO of the neutral radical is a simple system of p_z orbitals on alternating secondary carbon centers around the ring with a node at the center. The noninvolvement of the central atom in the SOMO makes it nearly impossible for ***P*** to form a simple sandwich structure to all six carbons in any one of its three six-membered rings or for a simple divalent metal such as Mg^{2+} to form an eclipsed or staggered (D_{3h} or D_{3d}) sandwich complex by bonding to the central atom of the rings.

Donald et. al.[17] previously examined and rationalized the bonding and thermodynamic stability in a series of sandwich complexes of the phenalenyl radical with divalent metals from across the periodic table. In that work, they showed that the radical is a versatile bonding partner as a ligand, and is, for example, sensitive to the size and shell structure of the metal atom than the simple cyclopentadienyl radical. The hapticity of the M***P***$_2$ complexes were found to evolve from η^1, η^3 for Be to η^6, η^6 for Ba going down Group

(17) Craciun, S.; Donald, K. J. *Inorg.Chem.* **2009**, *48*(13), 5810 - 5819.

2 and a similar diversity in bonding patterns was observed among the first-row d-block metals from Ca (η^6, η^6) to Cu (η^2, η^2) and Zn (η^1, η^1). They also found the nature of the frontier singly occupied molecular orbital (SOMO) of the radical to be crucial to rationalizing the diversity in the modes of metal phenalenyl coordination.

In this work, I analyze the thermodynamic and kinetic stability of main and d-block metal complexes with ***P*** in the forms of ***P***M and ***P***MX_n (M = Groups 1 and 11 metals and the early transition metals, Sc, Ti, V, and Cr and X = F, and Cl). The transition metals considered in this work were selected because simple cyclopentadienyl and benzene half sandwich complexes are known experimentally for those metals, and because some of those compounds, such as $TiCl_3$, $ScCl_2$, $V(CO)_4$, and others, are subjects of continuing interest as catalysts in known organic reactions.[18-34]

These phenalenyl half sandwich systems are especially interesting because the phenalenyl ring combines the structural properties of a six-membered benzene ring and the radical character of the cyclopentadienyl ring – in a relatively simple organometallic species. The high symmetry of ***P*** (D_{3h}) suggests that in cases where the barriers to

(18) Larkin, S. A.; Golden, J. T.; Shapiro, P. J.; Yap, G. P.' Foo, D. M.; Rheingold, A. L. *Organometallics*, **1996**, *15*(9), 2393–2398.
(19) Fridrichová, A.; Růžička, A.; Lamač, M.; Horáček, M. *Inorganic Chemistry Communications* **2017**, *76*, 62-66.
(20) Rehder, D.; Hoch, M.; Link, M. *Organometallics* **1988**, *7*(1), 233-235.
(21) Goto, K.; Kubo, T.; Yamamoto, K.; Nakasuji, K.; Sato, K.; Shiomi, D.; Ouyang, J. *J. Am. Chem. Soc.* **1999**, *121*(7), 1619-1620.
(22) Enders, M.; Fernández, P.; Ludwig, G.; Pritzkow, H. *Organometallics* **2001**, *20*(24), 5005-5007.
(23) Huang, Y.; Jin, G. *Dalton Trans*. **2009**, *5*, 767-769.
(24) Sassmannshausen, J.; Powell, A. K.; Anson, C. E.; Wocadlo, S.; Bochmann, M. *Journal of Organometallic Chemistry* **1999**, *592*(1), 84-94.
(25) Coville, N. J.; Plooy, K. E.; Pickl, W. *ChemInform* **2010**, *23*(47).
(26) Luo, Y.; Feng, X.; Wang, Y.; Fan, S.; Chen, J.; Lei, Y.; Liang, H. *Organometallics* **2011**, *30*(12), 3270-3274.
(27) Buijink, J. F.; Teuben, J. H.; Kooijman, H.; Spek, A. L. *Organometallics* **1994**, *13*(8), 2922-2924.
(28) Herberhold, M.; Kuhnlein, M.; Kremnitz, W.; Rheingold, A. L. *Journal of Organometallic Chemistry*. **1990**, *383*, 71-84.
(29) Kamegawa, T.; Saito, M.; Sakai, T.; Matsuoka, M.; Anpo, M. *Catalysis Today* **2012**, *181*(1), 14-19.
(30) Böhnke, J.; Braunschweig, H.; Jiménez-Halla, J. O.; Krummenacher, I.; Stennett, T. E. *J. Am. Chem. Soc.* **2018**, *140*(2), 848-853.
(31) Elschenbroich, C.; Salzer, A. Organometallics: a concise introduction. Weinheim: VCH **1992**.
(32) Djukic, J.; Rose-Munch, F.; Rose, E.; Simon, F.; Dromzee, Y. *Organometallics* **1995**, *14*(4), 2027-2038.
(33) Clark, I. P.; George, M. W.; Greetham, G. M.; Harvey, E. C.; Long, C. *et al. The Journal of Physical Chemistry A* **2011**, *115*(14), 2985-2993.
(34) Glans, L.; Taylor, D.; Kock, C. D. et al. *Journal of Inorganic Biochemistry* **2011**, *105*(7), 985-990.

translation across the surface of the tricyclic system are low, significant fluxional behavior may be observed. In this work, I report the outcomes of a series of investigations into the barriers to translation of the M and MX_n fragments across ***P***.

Computational Methods

The geometrical data, harmonic vibrational frequencies, and internal reaction coordinate (IRC) paths reported in this work have been obtained using the Becke three parameter hybrid functional b, with correlation provided by Perdew and Wang (the B3PW91 method)[35] as implemented in Gaussian 09 (G09) suite of programs[36]. The correlation-consistent triple-ζ (cc-pVTZ) basis sets were employed for all elements in the periodic table, except K, Rb, Cs, Ag and Au.[37] For the latter elements, the small core MDF pseudopotentials were employed along with the corresponding triple zeta basis sets for the higher energy electrons. 9-, and 19- valence electron effective core MDF pseudopotentials have been used, respectively, for the heavy group 1 metals (K, Rb, Cs) and group 11 metals (Ag, Au).[15] All molecular representations and images included in this article were generated using the Chemcraft graphical user interface[38] and the Chemdraw program. The Synchronous Transit-guided Quasi-Newton-Raphson method as implemented in the Gaussian 09 software- both the QST2 and QST3 options were employed to explore the nature of the trajectories to go between minima on the potential energy surface (PES) of ***P***ML_n complexes. In particular, the QSTn calculations enabled us to locate credible

(35) J. P. Perdew, in Electronic Structure of Solids, edited by P. Ziesche and H. Eschrig (Akademie Verlag, Berlin, **1991**)
(36) Frisch, M. J.; Trucks, G. W.; Schlegel, H. B.; Scuseria, G. E.; Robb, M. A.; Cheeseman, J. R.; Scalmani, G.; Barone, V.; Mennucci, B.; Petersson, G. A.; et al. Gaussian 09, Revision D.01; Gaussian, Inc.: Wallingford, CT, **2013**.
(37) Dunning, T. H. *J. Chem. Phys.* **1989**, *90*, 1007−1023.
(38) Chemcraft: Andrienko, A. G.; Senchenya, I. N.; Romanov, A.; http://www.chemcraftprog.com

candidate transition state structures linking minima on the PES. Candidate transition structures generated by QSTn analyses were confirmed by separate vibrational frequency calculations to be first order saddle points. A refined picture of each translation was accomplished by calculating IRC paths using the confirmed TS structures. The differences in the energies of each transition state structure and the fully optimized geometries of the IRC minima linked to each other by that TS have been calculated. The number of IRC data points was effectively unrestricted. We used very high "maxpoints" values such that the IRC path calculations terminated before any limit on the number of points was reached. Wiberg bond indices and other population analysis data that we report herein have been obtained from natural bond orbital (NBO) analyses on optimized geometries using the NBO 3.1 as implemented in the Gaussian 09 suite.

Results and Discussion

Two sets of complexes were considered in this work: a series of half sandwich (i) ***P***M complexes (M = Li, Na, K, Rb, Cs, Sc, Ti, V, Cr, Cu, Ag, and Au) and (ii) ***P***MX_n complexes where M = Sc, Ti, V, Cr, X = F, Cl and n = 2 when M = Sc and V, and n = 3 when M = Ti and Cr.

Close encounters of the third kind. Due to the size of ***P***, it is difficult for the M and MX_n fragments to bond symmetrically with the SOMO, which is restricted to alternating carbon sites on the large twelve carbon ring (Figure 1). We carried out a series of structural studies on these half sandwich complexes and observed significant variations in the structural preferences going across the row from Sc to Cr and down Groups 1 and

11. In most cases, the M and MX_n fragments coordinate to 2 or more atoms on ***P***. However, without a rigorous quantum mechanical classification, it is difficult to accurately identify each complexes' hapticity. That is, we are unable to derive meaningful results. We find that, as expected, the M-***P*** distances increase as M gets larger, and the following trends are observed:

i. The group 1, scandium and vanadium complexes as well as the Ti fragment all prefer the half-sandwich structure.

ii. The group 11, titanium and chromium complexes to bond directly to a single secondary C center.

Fluxionality. One expects low barriers to translation, leading to significant fluxional behavior due to the high symmetry of the ring (D_{3h}). To confirm this, we checked for the presence of multiple minima and attempted to elucidate the mechanisms for the translation (or hopping) of the M and MX_n fragments across the surface of the ring. We carried out IRC path calculations for all complexes. The IRC calculations were preceded by QSTn (n = 2 or 3) calculations that allowed us to obtain reasonable transitions states which were confirmed to be first-order saddle points. IRC path calculations were conducted using those confirmed structures. Figure 2 summarizes the different translational paths observed as well as the M and MX_n fragments that exhibited them. Figure 3 shows the IRC Pathways for the systems and movements shown in Figure 2.

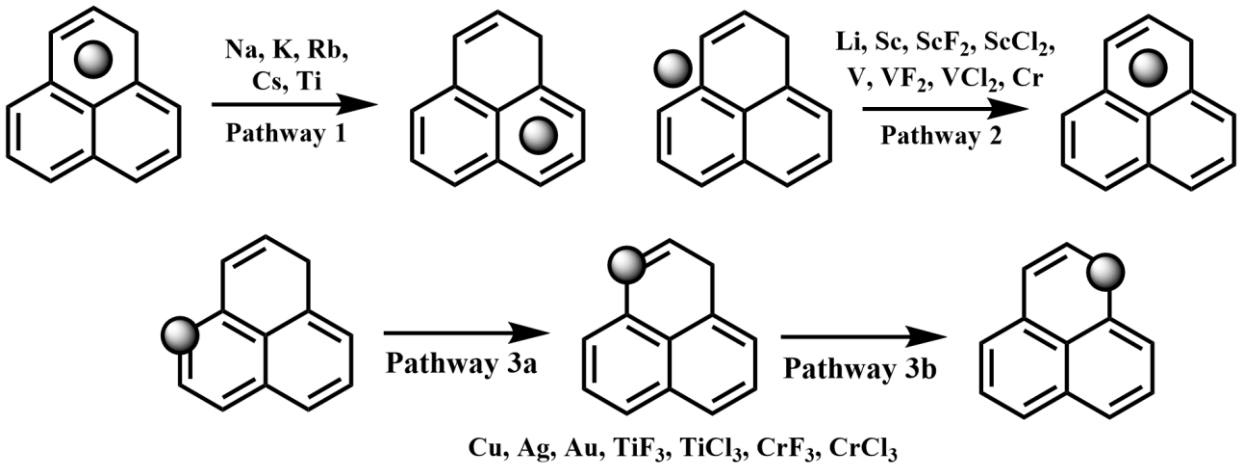

Figure 2. Summary of movements observed for the tested ***P***M (M = Li, Na, K, Rb, Cs, Sc, Ti, V, Cr, Cu, Ag, and Au) and ***P***MX_n complexes where M = Sc, Ti, V, Cr, X = F, Cl and n = 2 when M = Sc and V, and n = 3 when M = Ti and Cr. For clarity, all fragments are symbolized by a simple circle.

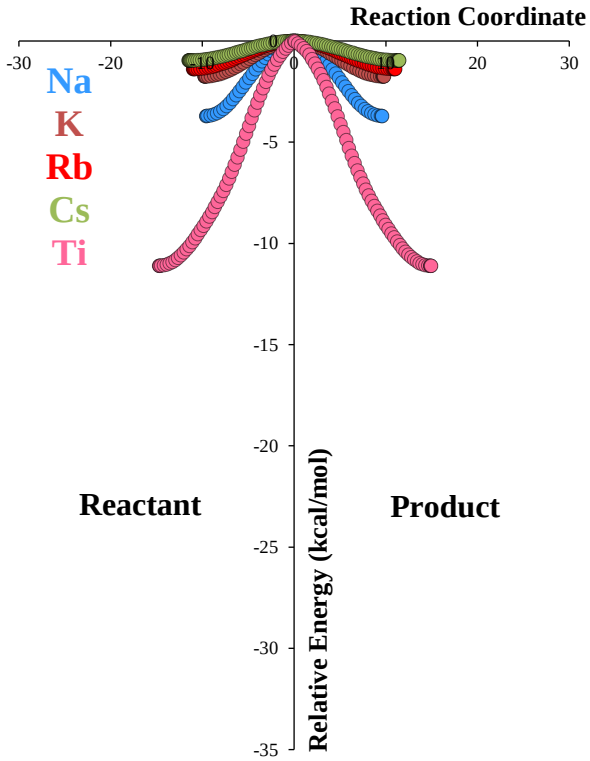

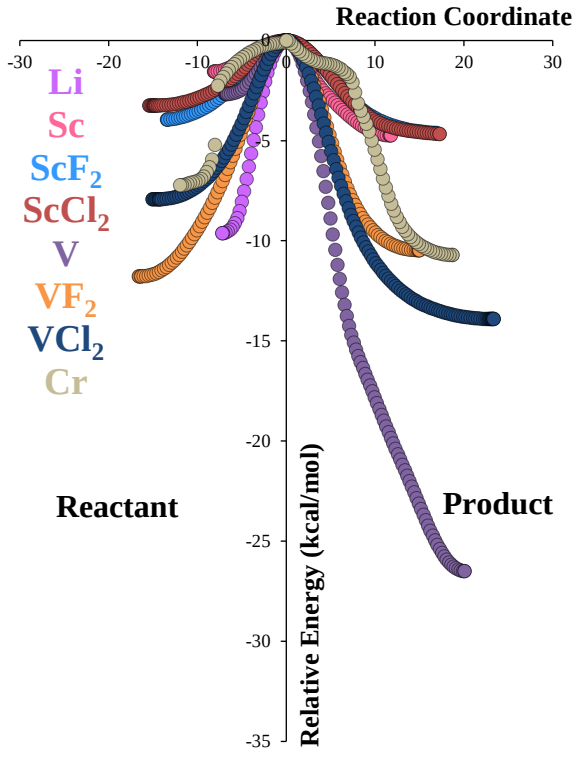

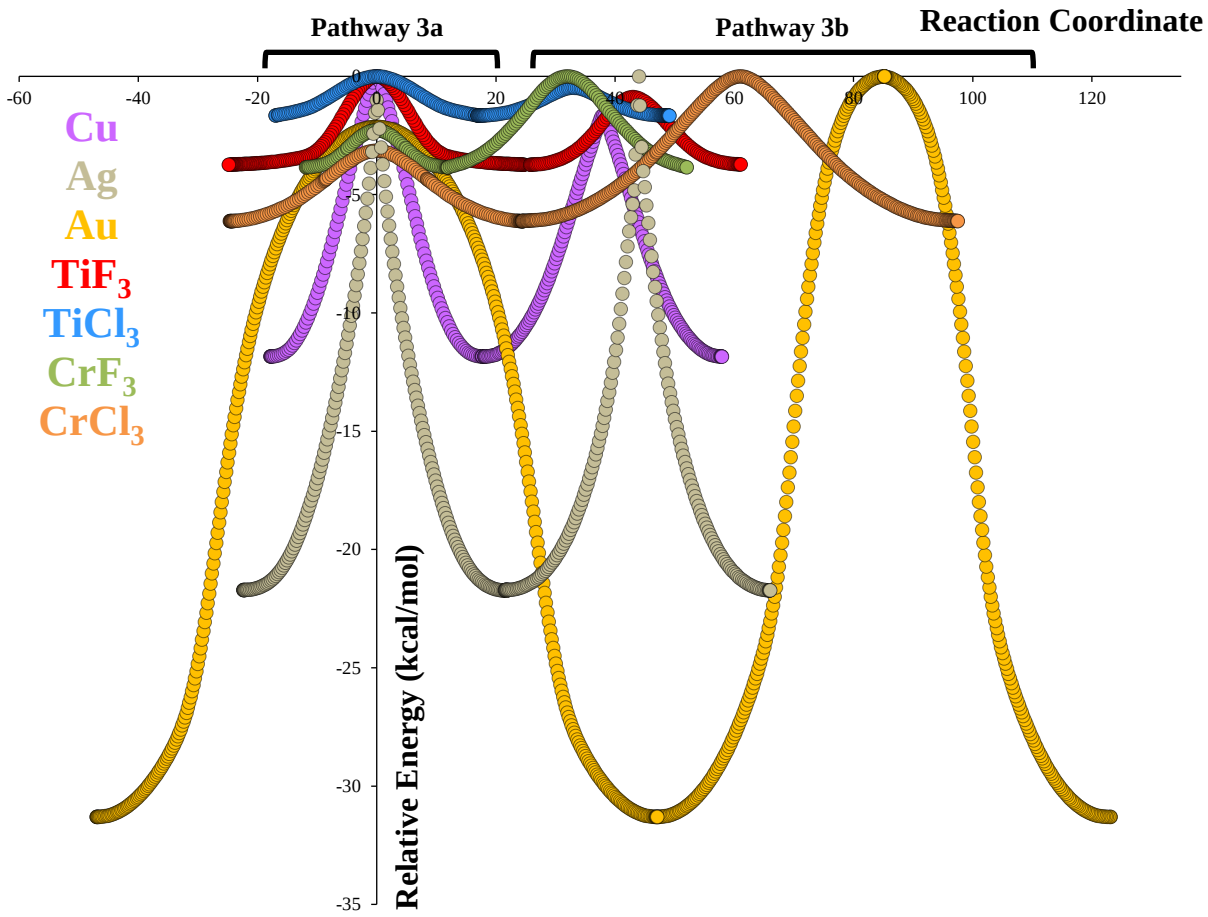

Figure 3. IRC graphs showing barriers to fluxionality of half sandwich complexes according to the different reaction Pathways. The top left graph shows Pathway 1, the top right graph shows Pathway 2 and the bottom IRC graphs shows Pathways 3a and 3b, respectively. For comparison, the four graphs are presented on the same vertical scale. The graphs should be read in the same order as Figure 2, i.e. the right half of each graph is the right half of each Pathway shown in Figure 2.

Quantifying the Barriers. The IRC paths do not necessarily terminate on either side of Figure 3 to fully optimized geometries, so we list in Tables 2 and 3 the differences in the free energies of the reactant (left) and product (right) of the translation. The free energy differences between those and the relevant transition state structures have been computed as well.

Pathway 1. As can be seen by the reaction Pathway in Figure 2, the reactant and

product in Pathway 1 can be assumed to be chemically equivalent. It is satisfying then to see that, although interacting with different parts of the ring, both positions are in fact identical. This is seen in Table 1 as there is no difference in energy between the reaction and product and the barriers on either side are the same. Therefore, it is fair to say the same energy barrier will exist for the next translational movement. We also find that Li is the only Group 1 metal that doesn't follow this Pathway. Conversely, Ti is the only transition metal fragment that follows Pathway 1. The energy barrier of ***P***Li, compared to the rest of the group, is most likely due to the fact that Lithium is the smallest Group 1 metal and bound very closely to the ring, requiring more energy to move it around the ring and displace it.

Pathway 2. Unlike Pathway 1, the reactant and product are chemically different (*the reactant is between two carbons on two separate rings, whereas the product is the half-sandwich complex*). For most of the fragments, the half-sandwich configuration is preferred – Li and VF_2 are the only exceptions. We find that barrier to fluxionality is indeed dependent upon the X_n bonded to the metal, and/or the metal itself. The compounds without any X_n bonded ended up having a significantly higher energy barrier than their X_n analogues. We find that the vanadium complexes have the highest energy barriers, going from the more stable product to the reactant. The energy barriers for the other structures were almost always below 5.5 kcal/mol, indicating high fluxionality. A surprising result is that although the IRC links the reactant and product, when optimized, Cr's product seems to be higher in energy than its transition state (by ~ 1.51 kcal mol^{-1}).

Pathway 3. Pathway 3 can be seen as a superficial combination of Pathways 1 and

2, as it encompasses translation across two rings and within a single ring. However, the fragments all bond directly to a single C center. While it is comforting to note that while the Pathway connects chemically equivalent configurations, it is unsurprising to see that in all but four cases, more energy is required to move across two rings than to move across a single ring.

Table 1. Free energy changes going from Reactant to Product (Δ Reactant − Product) and from the Product and Reactant to the Transition Structure (TS) of half sandwich ***P***M and ***P***MX_n complexes for the first two Pathways shown in Figure 2 calculated at the B3PW91 level of theory. A negative value means the right term in the equation is more stable.

Fragment	Reactant - Product	Reactant – Transition State	Product – Transition State
		Pathway 1	
Na	0.00	3.51	3.51
K	0.00	2.05	2.05
Rb	0.00	1.94	1.94
Cs	0.00	1.63	1.63
Ti	0.00	17.27	17.27
		Pathway 2	
Li	-7.59	8.76	1.16
Sc	4.51	0.84	5.35
ScF_2	0.57	3.94	4.51
$ScCl_2$	1.45	3.25	4.71
V	23.88	2.44	26.32
VF_2	-1.53	11.49	9.96
VCl_2	5.31	1.86	13.22
Cr	6.22	4.71	-1.51

Table 3. Free energy changes going from Reactant to Product (Δ Reactant − Product) and from the Product and Reactant to the Transition Structure (TS) of half sandwich ***P***M and ***P***MX_n complexes for the last Pathway shown in Figure 2 calculated at the B3PW91 level of theory. A negative value means the right term in the equation is more stable.

Fragment	Pathway 3a			Pathway 3b		
	Reactant - Product	Reactant – Transition State	Product – Transition State	Reactant - Product	Reactant – Transition State	Product – Transition State
Cu	0.00	11.26	11.26	0.00	9.32	9.32
Ag	0.00	19.62	19.62	0.00	20.25	20.25
Au	0.00	28.24	28.24	0.00	30.05	30.05
TiF_3	0.00	5.65	5.56	0.00	4.45	4.45
$TiCl_3$	0.00	3.16	3.16	0.00	2.12	2.12
CrF_3	0.00	1.50	1.50	0.00	5.00	5.00
$CrCl_3$	0.00	2.85	2.85	0.00	6.48	6.48

Summary and Future Considerations

In this work, I have carried out a series of investigations into the fluxionality of phenalenyl complexes. I find that going down group 1, the energy barriers get lower, i.e. bigger the elements get, the more fluxional these systems seem to be, with all energy barriers outside of Li being under 5 kcal/mol. The reverse seems to be the true for the group 11 complexes, as the energy barrier of Au towers over that of Ag and Cu.

For further research, I wish to continue analyzing bigger polycyclic rings comprising primarily of carbons and hydrogens, eventually working our way up to molecules like graphene, to see how we can move things across the surfaces of planar carbon. Also, we want to see the potential of these highly fluxional complexes as catalysts, specifically for olefin polymerizations, and seeing what sort of activity the phenalenyl ring can have.

Investigations into σ-hole Interactions and Consequences for Structure

Introduction

The concept of a σ-hole was developed by Clark et al. within the context of halogen bonding.[39] In that work, they describe a σ-hole as a region of positive electrostatic potential on the outermost portion of a halogen's (X) surface, centered on the R-X axis. This explanation also accounts for the remarkable directionality of halogen bonding: the angle R—X - - - base is usually close to (if not exactly) 180°. However, this description is insufficient as it limits the origin of σ-holes to strictly halogen bonds. However, this is not the case. A more appropriate definition of a σ-hole is an electron-deficient outer lobe of a half-filled p- (or nearly p-) orbital involved in the formation of a covalent bond, as shown in Figure 4. If the electron deficiency is sufficient, a region of positive electrostatic potential will result,[40,41,42] which can then interact attractively (and noncovalently) with negative sites on other molecules.

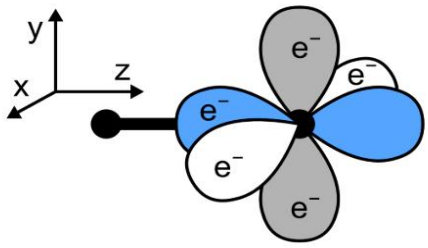

Figure 4. Sample orbital arrangement. The p_x (white), p_y (gray), and p_z (blue) valence orbitals on an atom. The outer half of the p_z valence orbital is electron-deficient, which expresses itself as a σ-hole.[43]

(39) Clark, T.; Hennemann, M.; Murray, J. S.; Politzer, P. *J. Mol. Model.* **2007**, *13*, 291.
(40) Brinck, T.; Murray, J. S.; Politzer, P. *Int. J. Quantum Chem., Quantum Biol. Symp.* **1992**, *19*, 57.
(41) Murray, J.S.; Paulsen, K.; Politzer, P. *Proc. Indian Acad. Sci. (Chem. Sci.)* **1994,** *106*, 267.
(42) Auffinger, P.; Hays, F.A.; Westhof, E.; Shing, Ho P. *PNAS* **2004**, *101*, 16789–16794.
(43) Kolář, M. H.; Hobza, P. *Chemical Reviews* **2016**, *116*(9), 5155-5187.

σ-hole interactions have been well studied for many covalently-bonded atoms of Groups V–VII. [44,45,46] It has been found that the positive character of the σ-hole increases going from the lighter to the heavier (more polarizable) atoms down a group, and as the remainder of the molecule becomes more electron-withdrawing.[46] As a result, it has become increasingly useful to create molecular electrostatic surface potential maps to quantify sigma holes as shown in Figures 5 and 6. The most commonly used electron density was proposed by Bader et al. - 0.001 au (i.e., e/bohr^3),[47] which encompasses approximately 96% of the electronic charge of a molecule. It is worth noting that although σ holes are uncommon on bonded fluorines, they are not unknown.[48,49]

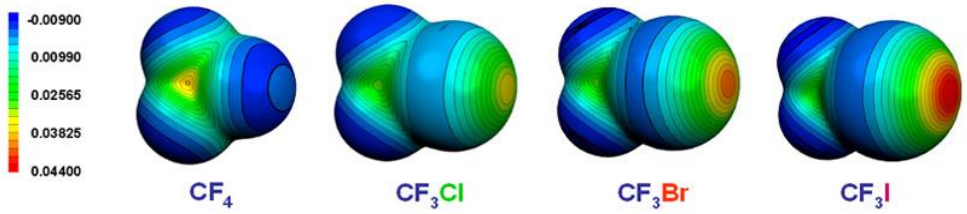

Figure 5. Molecular electrostatic surface potential of CF_4, CF_3Cl, CF_3Br and CF_3I.[39] The σ-hole is signified by the red disc.

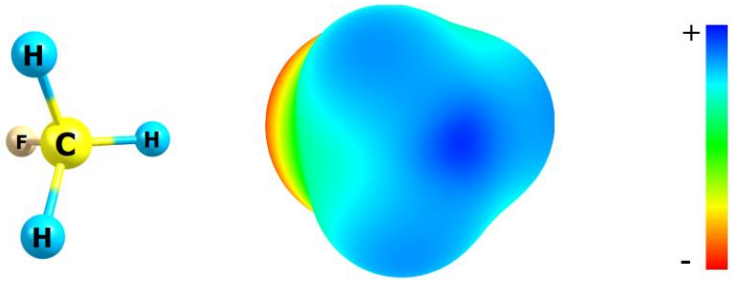

Figure 6. The ball-stick model of fluoromethane (*left*). The blue disc on the molecular electrostatic potential surface represents the σ-hole.

(44) Guo, N.; Maurice, R.; Teze, D.; Graton, J.; Champion, J.; Montavon, G.; Galland, N. *Nature* **2018**, *10*(4), 428-434.
(45) Pal, R.; Nagendra, G.; Samarasimhareddy, M.; Sureshbabu, V. V.; Row, T. N. *Chem. Commun.* **2015**, *51*, 933-936.
(46) Murray, J. S.; Lane, P.; Politzer, P. *Journal of Molecular Modeling* **2008**, *15*(6), 723-729.
(47) Bader, R. F.; Carroll, M. T.; Cheeseman, J. R.; Chang, C. *J. Am. Chem. Soc.* **1987**, *109*, 7968–7979.
(48) Politzer, P.; Murray, J.S.; Concha, M.C. *Journal of Molecular Modeling* **2007**, *13*(6–7), 643–650.
(49) Wang, Y. H.; Lu, Y. X.; Zou, J. W.; Yu, Q. S.; *Int. J. Quantum Chem.* **2008**, *108*, 1083–1089.

As previously mentioned, σ-hole interactions are highly directional,[40,50] that is to say, σ-holes represent a structure-determining force, and the nearly linear arrangement is a consequence. Certainly, the broad applications of halogen bonding in biosciences and material sciences owe its functionality to it.[51,52] But the question certainly arises: to what extent does a linear arrangement strengthen the σ-hole interaction? One of the most important features of σ-hole interactions is their binding energy, the energy that is released upon formation of the bond or is needed to break it:

$$\Delta E_{binding} = E_{complex} - E_{fragment1} - E_{fragment2}$$

The greater the binding energy, the stronger the σ-hole interaction is said to be. Unfortunately, the total binding energy fails to tell us which energy component is dominant. This information is not only important for understanding the nature of bonding but also for optimizing/maximizing the strength of the respective σ-hole interaction.

In this work, I investigate the effect of directionality on the σ-hole interaction between M-F (M = Li, Na, K, Cu, Ag, Au) compounds and well-known electron donors (D = BF and NH_3) by determining their binding energies as the <DMF angle changes. By changing the <DMF angle and determining the binding energy, I am able to evaluate and comment on the dependency of a linear arrangement on the overall stabilization of a complex. I also perform energy decomposition analysis on each complex at the different geometries to to determine which energy contribution (and repulsion) is dominant.

(50) Politzer, P.; Lane, P.; Concha, M. C.; Ma, Y.; Murray, J. S. *Journal of Molecular Modeling* **2007**, *13*, 305-311.
(51) Politzer, P.; Murray, J. S.; Clark, T. *Phys. Chem. Chem. Phys.* **2010**, *12*, 7748– 7757.
(52) Cavallo, G.; Metrangolo, P.; Milani, R.; Pilati, T.; Priimagi. T.; Resnati, G.; Terraneo, G. *Chem. Rev.* ***2016***, *116* (4), 2478–2601.

Computational Methods

The extended transition state - natural orbitals for chemical valence (ETS-NOCV)[53,54] analysis was done based on the Amsterdam Density Functional (ADF) package[55,56,57] in which this scheme was implemented. The Becke, three-parameter, Lee-Yang-Parr[58,59,60]exchange-correlation functional (B3LYP) along with the TZP basis set was applied for all atoms.[61] Geometry optimizations and vibrational frequency analyses[62,63,64,65,66] of the configurations were also calculated and the zero-order regular approximation (ZORA) basis set[67] was used where relativistic effects were considered. The <DMF angle was changed in 5° increments from 180° to 90°, keeping the interatomic distances constant, according to Figure 7.

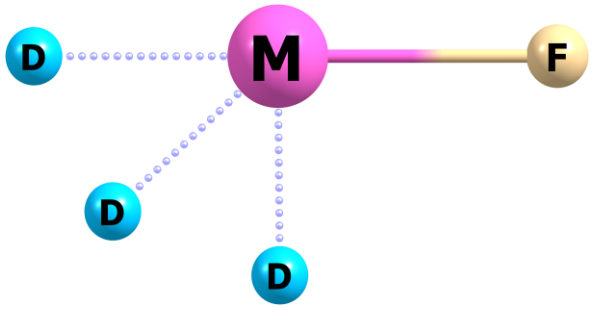

Figure 7. Diagrammatic representation of the change in <DMF angle while keeping the interatomic distances constant.

(53) Ziegler, T.; Rauk, A. *Theoretica chimica acta* **1977**, *45*, 1-10.
(54) Bickelhaupt, F. M.; Baerends, E. J. In: Reviews in Computational Chemistry Vol. 15 **2000**.
(55) Velde, G.te; Bickelhaupt, F.M.; Baerends, E.J.; Fonseca, G. C.; van Gisbergen, S. J. A.; Snijders, J.G.; Ziegler, T. *Journal of Computational Chemistry* **2001**, *22*, 931.
(56) Fonseca, G. C.; Snijders, J.G.; Velde, G. te; Baerends, E.J. *Theoretical Chemistry Accounts* **1998**, *99*, 391.
(57) ADF2013, SCM, Theoretical Chemistry, Vrije Universiteit, Amsterdam, The Netherlands, http://www.scm.com.
(58) Becke, A. D. *Phys. Rev. A.* **1988**, *38*(6), 3098–3100.
(59) Lee, C.; Yang, W.; Parr, R.G. *Phys. Rev. B.* **1988**, *37*(2), 785–789.
(60) Becke, A. D. *J. Chem. Phys*. **1993**, *98*(7), 5648–5652.
(61) van Lenthe, E.; Baerends, E. J. *Journal of Computational Chemistry* **2003**, *24*, 1142.
(62) Fan, L.; Ziegler, T. *Journal of Chemical Physics* **1992**, *96*, 9005.
(63) Fan, L.; Ziegler, T. *Journal of Physical Chemistry* **1992**, *96*, 6937.
(64) Bérces, A.; Dickson, R. M.; Fan, L.; Jacobsen, H.; Swerhone, D.; Ziegler, T. *Computer Physics Communications* **1997**, *100*, 247.
(65) Jacobsen, H.; Bérces, A.; Swerhone, D.; Ziegler, T. *Computer Physics Communications* **1997**, *100*, 263.
(66) Wolff S. K. *Journal of Quantum Chemistry* **2005**, *104*, 645.
(67) Rosa, A.; Baerends, E.J.; van Gisbergen, S. J. A.; van Lenthe, E.; Groeneveld, J. A.; Snijders, J. G. *Journal of the American Chemical Society* **1999**, *121*, 10356.

Results and Discussion

The effect of directionality on the σ-hole interaction between M-F (M = Li, Na, K, Cu, Ag, Au) compounds and well-known electron donors (D = BF and NH_3) as the <DMF angle changes has been investigated. However, we must first consider the size and magnitude of the sigma-hole present on the metals, shown in Figure 8. We find that although M = Li possesses the largest and most positive sigma-hole, all the metals considered in this work possess a sigma hole, with the lowest potential being approximately +0.0919 au. We also find that both donors clearly possess a region of negative potential, due to increased electron density presence on the B and N in BF and NH_3, respectively.

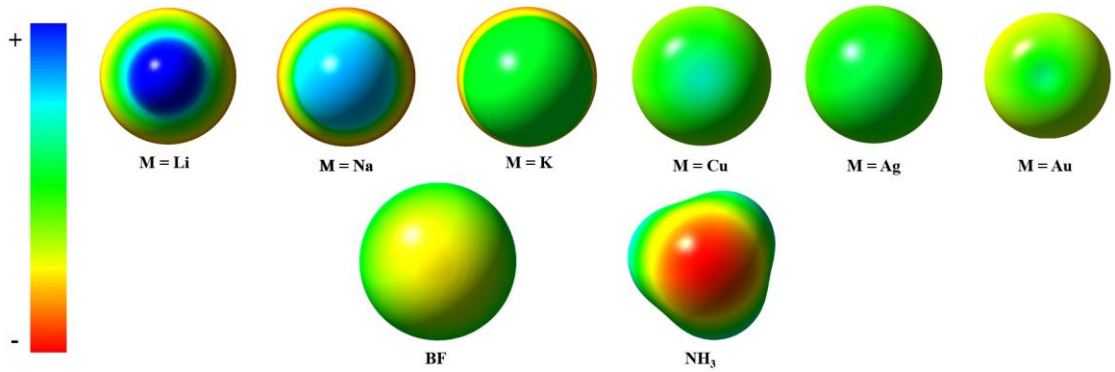

Figure 5. Molecular electrostatic surface potential showing σ holes of MF (M = Li, Na, K, Cu, Ag, Au) and electron rich region of BF and NH_3 calculated at 0.001 au electron density surface at the B3LYP/cc-pVTZ level. Each MF surface was standardized to Li's scale. NH_3 and BF were standardized to NH_3's scale.

For the systems considered in this work, the optimized D---M bond distances as well as the dipole moments of MF are shown in Table 1. The dipole moments follow the general trends expected, reflecting the decrease in electronegativity in Group 1 and the subsequent increase going down Group 11. The dipole moment of AuF could not be found in the literature. The computed bond distances also follow the general trends as expected, reflecting the increasing size of M and the decrease in size of B → N as we descend each

group. However, an interesting feature of the structural data is that of the Group 11 metals, Ag, not Au, exhibits the largest M---D distance. This might be a consequence of the shell structure or lanthanide contraction in Au; however, we do not attempt to answer this phenomenon in this work.

Table 3. Table showing the dipole moments of the compounds considered in this work as well as the optimized FM---D distances for M = Li, Na, K, Cu, Ag and Au and D = BF and NH_3. No known dipole moment could be found for BF, however the dipole moment for NH_3 is known to be 1.4718 ± 0.0002 μ/D.

Metal	Dipole Moment (μ/D) [68,69,70]	FM--BF Distance	FM--NH_3 Distance
Li	6.3274 ± 0.0002	2.38	2.05
Na	8.156 ± 0.001	2.78	2.43
K	8.585 ± 0.003	3.53	3.12
Cu	5.77 ± 0.29	1.83	1.93
Ag	6.22 ± 0.30	1.96	2.14
Au	-	1.87	2.07

Figures 6 and 7 show the binding energies of the FM---D systems for NH_3 and BF, respectively. The graphs show, except in the case of FK, for both donors, and FNa---BF, the systems are at their most stable when the <FMD is approximately close or exactly equal to 180. We find that the Au---D interaction is most strengthened by a linear geometry (up to -55 kcal/mol), and that the linear geometry of FLi---D is the most stable of the group 1 systems considered for both donors (up to -9 kcal/mol).

(68) *Landolt-Börnstein, Numerical Data and Functional Relationships in Science and Technology, New Series*, II/6 (**1974**), Springer-Verlag, Heiderlberg.
(69) *Landolt-Börnstein, Numerical Data and Functional Relationships in Science and Technology, New Series*, II/14a (**1982**), Springer-Verlag, Heiderlberg.
(70) *Landolt-Börnstein, Numerical Data and Functional Relationships in Science and Technology, New Series*, II/19c (**1992**), Springer-Verlag, Heiderlberg.

The bonding analysis presented in this study is based on the ETS-NOCV approach, implemented in ADF, which is a combination of the extended transition state (ETS) method with the natural orbitals for chemical valence (NOCV) scheme. In our analysis, each system is divided up into two individual fragments as shown schematically by purple vertical lines in Figure 8. We used the ETS-NOCV method to study the interaction between these subsystems. In the ETS energy decomposition scheme, the interaction energy ΔE_{int} between the fragments (exhibiting geometries as in the combined molecule) is divided into three components:

$$\Delta E_{int} = \Delta E_{elstat} + \Delta E_{Pauli} + \Delta E_{orb}$$

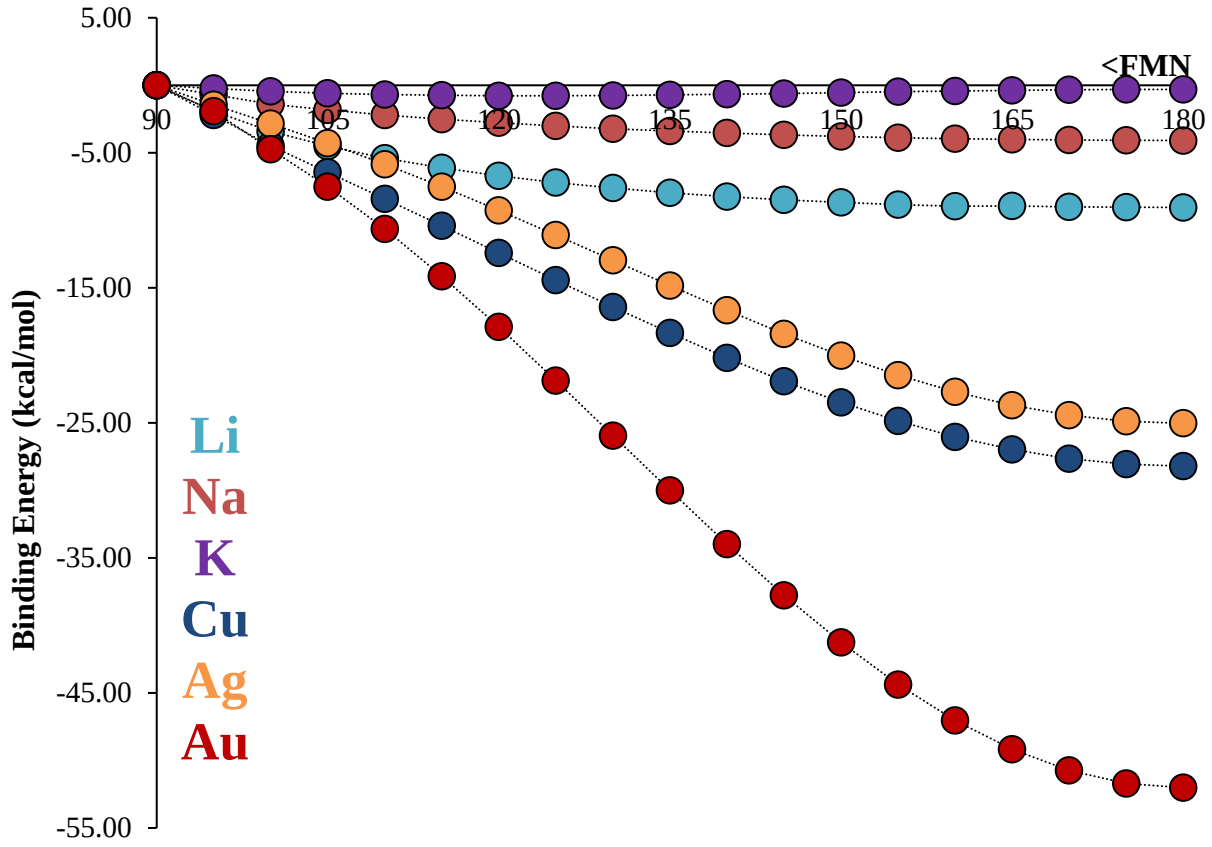

Figure 6. The binding energy profiles of MF complexes (M = Li, Na, K, Cu, Ag, Au) with NH_3 calculated at the B3LYP/TZP level.

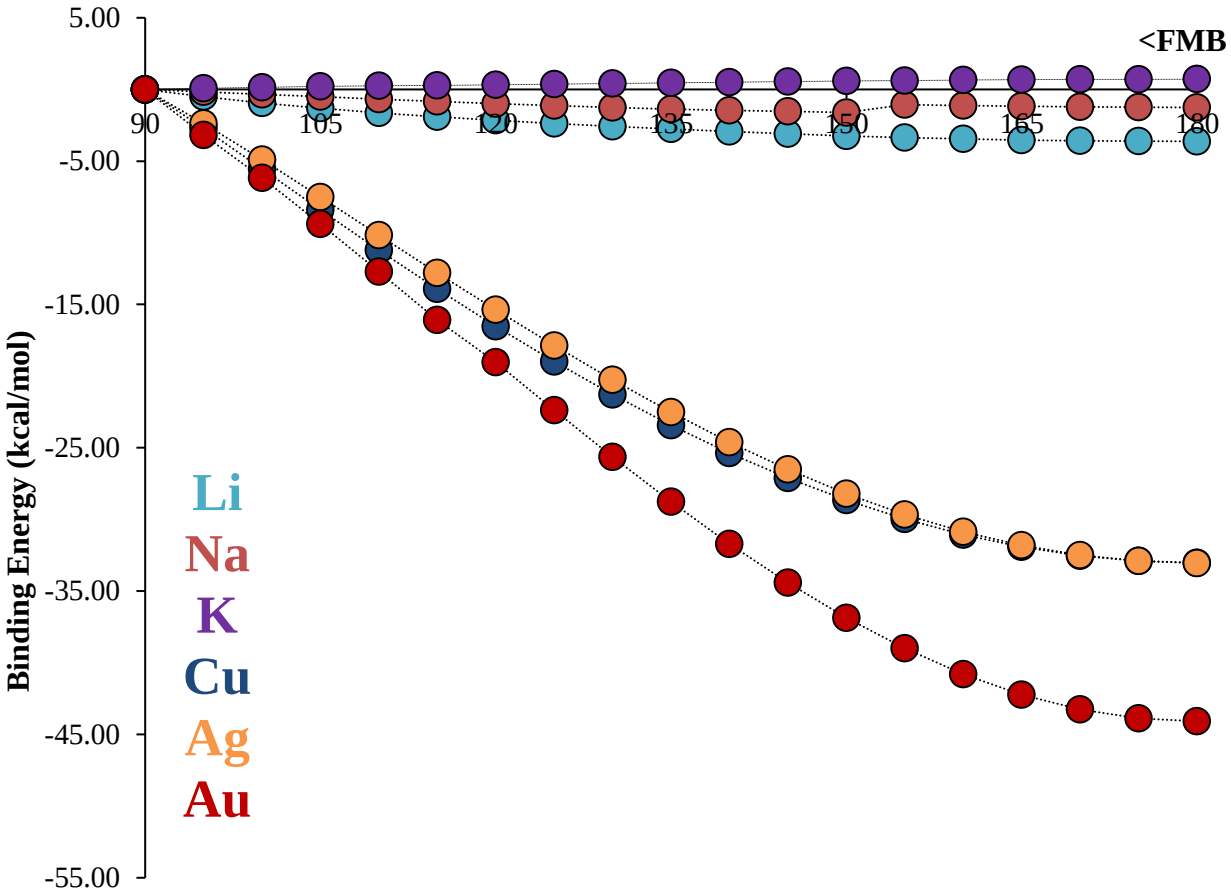

Figure 7. Binding energy profiles of MF complexes (M = Li, Na, K, Cu, Ag, Au) with BF calculated at the B3LYP/TZP level.

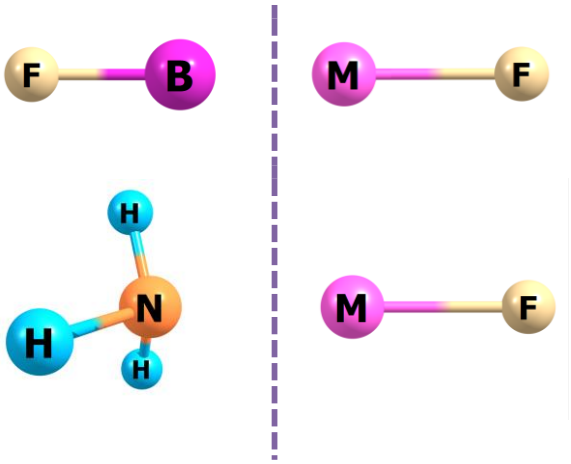

Figure 8. Decomposition scheme according to the ETS-NOCV method as implemented in ADF.

The first term, ΔE_{elstat}, corresponds to the classical electrostatic interaction between the fragments as they are brought to their positions in the final molecule. The second term,

ΔE_{Pauli}, accounts for the repulsive Pauli interaction between occupied orbitals on the fragments in the combined molecule. The third stabilizing term, ΔE_{orb}, represents the interactions between the occupied molecular orbitals of one fragment with the unoccupied molecular orbitals of the other fragments as well as mixing of occupied and virtual orbitals within the same fragment (inner-fragment polarization). This energy term may be linked to the electronic bonding effect coming from the formation of a chemical bond. It is necessary to mention at this point that the total orbital interaction term includes the inter-fragments electron flow as well as the intra-fragment polarization; thus, depending on the terminology used it could be considered as the polarization energy component.[51,71,72] I find that that the most dominant attractive and repulsive interactions are the electrostatic interaction (ΔE_{elstat}) and the exchange (Pauli) repulsion (ΔE_{Pauli}), respectively. As the <DMF $\rightarrow 90^{o}$, we find that the ΔE_{elstat} decreases across all metals for both donors, whereas the opposite is true for Ag and Au. The ΔE_{Pauli} increases as <DMF $\rightarrow 90^{o}$, for across all metals for both donors, except for K with NH_3.

Summary and Future Considerations

In this work, I have investigated and reported the effect of directionality on the σ-hole interaction between M-F (M = Li, Na, K, Cu, Ag, and Au) compounds and well-known electron donors (D = BF and NH_3). Results indicate that the sigma-hole interaction is significantly strengthened by a linear geometry (upto 55 kcal mol^{-1}), except in the case of

(71) Chen, J.; Martinez, T. J.; QTPIE: *Chem. Phys. Lett.* **2007**, *438*, 315–320.
(72) Sokalski, W. A.; Roszak, S. M. *J. Mol. Struct. THEOCHEM*, **1991**, *80*, 387–400.

KF with either donor. Energy decomposition analyses shows the dominant attractive and repulsive energy contributions to be the electrostatic interaction (ΔE_{elstat}) and the exchange (Pauli) repulsion (ΔE_{Pauli}), respectively. In future research, it may be worthwhile to study the effect of the linear geometry using other, popular Lewis bases, such as H_2O and a more exhaustive list of Lewis acids (such as CF_3X, where the σ-hole is on the X halogen).